Rme-8 depletion perturbs Notch recycling and predisposes to pathogenic signaling

Maria J. Gomez-Lamarca,[1]* Laura A. Snowdon,[1]* Ekatarina Seib,[2] Thomas Klein,[2] and Sarah J. Bray[1]

[1]Department of Physiology, Development and Neuroscience, University of Cambridge, Cambridge CB2 3DY, England, UK
[2]Institute of Genetics, Heinrich Heine University Düsseldorf, 40225 Düsseldorf, Germany

Notch signaling is a major regulator of cell fate, proliferation, and differentiation. Like other signaling pathways, its activity is strongly influenced by intracellular trafficking. Besides contributing to signal activation and down-regulation, differential fluxes between trafficking routes can cause aberrant Notch pathway activation. Investigating the function of the retromer-associated DNAJ protein Rme-8 in vivo, we demonstrate a critical role in regulating Notch receptor recycling. In the absence of Rme-8, Notch accumulated in enlarged tubulated Rab4-positive endosomes, and as a consequence, signaling was compromised. Strikingly, when the retromer component *Vps26* was depleted at the same time, Notch no longer accumulated and instead was ectopically activated. Likewise, depletion of ESCRT-0 components *Hrs* or *Stam* in combination with *Rme-8* also led to high levels of ectopic Notch activity. Together, these results highlight the importance of Rme-8 in coordinating normal endocytic recycling route and reveal that its absence predisposes toward conditions in which pathological Notch signaling can occur.

Introduction

The highly conserved Notch signaling pathway is a key regulator of many developmental decisions, controlling processes such as proliferation and differentiation. Inappropriate pathway activation is associated with several human diseases, including hematopoietic and solid tumors (Lobry et al., 2011). As a consequence, tight spatiotemporal regulation of Notch activity is essential. Intracellular trafficking is an important element in such regulation, influencing steps involved in signal activation as well as in preventing inappropriate signaling (Brou, 2009).

In canonical signaling, Notch is activated by ligands of the DSL (Delta [Dl], Serrate, Lag-2) family presented by neighboring cells. Upon ligand binding, Notch undergoes two consecutive proteolytic cleavages, catalyzed by an ADAM (A Disintegrin And Metalloproteinase) metalloprotease (S2 cleavage) and the γ-secretase complex (S3 cleavage). The latter releases the Notch intracellular domain (NICD) from the membrane, which translocates to the nucleus, where it regulates transcription of a variety of target genes (Bray, 2006). Signaling is highly sensitive to levels, localization, and modifications of the membrane proteins, which in turn are dependent on vesicular trafficking routes. For example, regulated trafficking is important for active ligand function and for turnover of inactive Notch receptors (Brou, 2009). In addition, ligand-independent trafficking of the full-length receptor to the late endosome and lysosome can result in activation (Fortini and Bilder, 2009). In *Drosophila melanogaster*, the ring finger protein Deltex (Dx) is one factor that promotes signaling via this alternate late-endosomal mechanism, which, like ligand induced activation, relies on γ-secretase–mediated cleavage (Baron, 2012).

For endocytosed cargoes to reach the correct final destination, they have to be sorted into distinct endosomal compartments (e.g., Fig. S3 K). A significant fraction of endocytosed Notch is transferred into intraluminal vesicles (ILVs) of so-called multivesicular bodies (MVBs), destined for degradation once MVBs fuse with lysosomes (Henne et al., 2011). The sorting and internalization of cargoes into ILVs is performed by endosomal sorting required for transport (ESCRT) complexes. Mutations affecting this process result in Notch being retained in the limiting membrane of MVBs where conditions facilitate proteolytic release of NICD, resulting in ectopic signaling (Moberg et al., 2005; Thompson et al., 2005; Vaccari and Bilder, 2005; Vaccari et al., 2008; Hori et al., 2011)

Besides being routed to lysosomes for degradation, internalized proteins can be recycled back to the plasma membrane or transferred to the Golgi. Early endosomes, marked by Rab5 GTPase, are the hub where internalized cargoes are sorted into different domains depending on their destination. For example, Rab4 marks a tubular subdomain of early endosomes that is involved in rapid recycling of cargoes to the plasma membrane.

*M.J. Gomez-Lamarca and L.A. Snowdon contributed equally to this paper.

Correspondence to Sarah J. Bray: sjb32@cam.ac.uk

Abbreviations used in this paper: Ci, Cubitus interruptus; Dl, Delta; D/V, dorsoventral; Dx, Deltex; *en*, *engrailed*; ESCRT, endosomal sorting required for transport; ILV, intraluminal vesicle; Kuz, Kuzbanian; MVB, multivesicular body; NECD, Notch extracellular domain; NICD, Notch intracellular domain; NRE, Notch responsive element; Ri, RNAi; Su(dx), Suppressor of Dx; TEM, transmission EM; UAS, upstream activation sequence; Wg, Wingless; WT, wild type.

The Rockefeller University Press $30.00
J. Cell Biol. Vol. 210 No. 2 303–318
www.jcb.org/cgi/doi/10.1083/jcb.201411001

Cargoes destined for recycling are concentrated in tubular extensions through the actions of complexes, including retromer (Jovic et al., 2010). First identified as a result of its role in retrograde transport from early endosomes to trans-Golgi, retromer is also involved in direct endosome-to-plasma membrane transport of proteins such as the β2-adrenergic receptor (Seaman, 2012; Seaman et al., 2013). It consists of two subcomplexes, a cargo-sorting subcomplex, composed of Vps35/Vps26/Vps29, and a sorting nexin subcomplex, which promotes tubulation (McGough and Cullen, 2011). The associated proteins include the Rme-8 (receptor-mediated endocytosis-8), a member of the DNAJ (J-domain containing) protein family of co-chaperones, whose absence leads to highly branched endosomal tubules and missorting of cargoes (Popoff et al., 2009; Shi et al., 2009; Freeman et al., 2014). Indeed, pathogenic mutations in *Rme-8* and in *Vps35* have been found in some instances of familial Parkinson's disease, underscoring the importance of endosomal recycling pathways (Vilariño-Güell et al., 2011, 2014).

First identified as a protein required for endocytosis in *Caenorhabditis elegans* (Girard et al., 2005), evidence now indicates that Rme-8 is primarily involved in postendocytic transport steps. Although the Hsc40-binding DNAJ domain is the only obvious feature of its sequence, biochemical studies have shown that the mammalian protein can bind to retromer components (SNX1) and WASH complex (the major endosomal actin polymerization-promoting complex) through other parts of the protein (Popoff et al., 2009; Shi et al., 2009; Freeman et al., 2014). Rme-8 may therefore link together requisite elements of the transport machinery in endocytic tubules (Freeman et al., 2014), but it remains to be established what role the DNAJ domain or Hsc40 play in this process.

Although previous studies have not detected a requirement for retromer in normal Notch function (Belenkaya et al., 2008; Franch-Marro et al., 2008; Pocha et al., 2011), our small scale screen for factors influencing Notch, along with larger screens by others (Le Bras et al., 2012), identified *Rme-8* as a potential regulator. Therefore, we have investigated here the role of Rme-8 in Notch trafficking and in the organization of the endosomal network in vivo. Our results indicate that Rme-8 is necessary for normal Notch recycling. Furthermore, they reveal that reductions in *Rme-8* sensitize the cells so that additional loss of sorting retromer or ESCRT-0 components have catastrophic effects. The fact that such synthetic combinations result in ectopic Notch activity and tissue overgrowth has major implications in the context of human disease mutations affecting *Rme-8* and related genes.

Results

Rme-8 is a positive regulator of the Notch pathway

In a small-scale genetic screen, using an *RNAi* (*Ri*) collection against known trafficking proteins, we identified the DNAJ protein Rme-8 as a positive modulator of the Notch pathway. *Rme-8* knockdown at late stages of wing development (using sal^{EPv}*-Gal4* to express *Rme-8 Ri*; Fig. 1 A; Cruz et al., 2009) gave rise to wings with thickened veins (L2 and L3) and, occasionally, small deltas (Fig. 1 C, arrows). This phenotype is reminiscent of reduced Notch function as illustrated by phenotypes produced when the Notch pathway transcription factor, Su(H), was perturbed using the same conditions (Fig. 1 D). Additional defects, such as posterior vein loss and more severe changes in wing morphology were also observed, indicating that Rme-8 has Notch-independent roles (Fig. 1 C, arrowhead). However, the penetrance of the vein thickening phenotypes suggests that the Notch pathway may be particularly sensitive to *Rme-8* depletion.

To verify that *Rme-8* depletion affected Notch activity, we assessed the consequences on a Notch responsive element (NRE) reporter, *NRE-mCherry*, when *Rme-8-Ri* was expressed in the posterior domain of wing imaginal discs (using *engrailed* [*en*]*-Gal4*; Fig. 1 E). Normally, NRE-mCherry is strongly expressed in a stripe along the dorsoventral (D/V) boundary with lower levels in flanking inter-vein regions (Fig. 1 F; Housden et al., 2012). Knockdown of *Rme-8* (Fig. S1 A) led to reduced NRE-mCherry expression, both at the D/V boundary and in surrounding regions (Fig. 1, G and J), although to a substantially lesser extent than depletion of *Su(H)* in the same way (Fig. 1 H). In these (and subsequent experiments), similar phenotypes were obtained using two independent Ri lines that target different regions in *Rme-8* transcripts ($Rme\text{-}8^{KK}$ *Ri* and $Rme\text{-}8^{GD}$ *Ri*, the former gave slightly stronger phenotypes). Likewise, *NRE-mCherry* expression was reduced in clones of *Rme-8* mutant cells, generated with a previously described x ray–induced loss-of-function allele ($Rme\text{-}8^{C19}$; Fig. 1, I and J; Chang et al., 2004). Together, these data indicate that Rme-8 is required for full Notch pathway activity and that it normally acts as a positive regulator of Notch function.

Aberrant Notch and Wingless (Wg) localization in the absence of Rme-8

Because Rme-8 is an evolutionary conserved endosomal-associated protein (Zhang et al., 2001; Chang et al., 2004; Girard et al., 2005; Fujibayashi et al., 2008; Girard and McPherson, 2008; Popoff et al., 2009; Shi et al., 2009), it likely affects Notch signaling by altering trafficking of key pathway components. We therefore investigated the consequences of *Rme-8* knockdown on the distribution of Notch and its ligand, Dl. Both proteins accumulated together in enlarged intracellular puncta in *Rme-8*–depleted territories (Fig. 2 A, arrowheads), demonstrating that Rme-8 is required for proper Notch and Dl trafficking. Concomitant with the increase in intracellular accumulation, their levels at the plasma membrane were decreased (Fig. 2, A–D; and Fig. S1 B). Furthermore, the intracellular puncta contained both intracellular (NICD) and extracellular domains of Notch (Notch extracellular domain [NECD]), suggesting that the uncleaved form of the receptor accumulates upon *Rme-8* depletion (Fig. 2, B–B″, arrowheads). Similar intracellular Notch puncta were also present in *Rme-8* mutant cells (Fig. 2 E, $Rme\text{-}8^{C19}$; and Fig. S1 C, $Rme\text{-}8^{A9}$). Although both Notch and Dl were affected, the reduced signaling appeared autonomous to *Rme-8*–depleted cells, suggesting that the receptor is particularly compromised (rather than the ligand). Phenotypes in the ovary also indicated a requirement for *Rme-8* in signal receiving follicle cells rather than the signal-sending oocyte (unpublished data) arguing that the primary defect arises from changes to Notch function.

Although adult phenotypes were reminiscent of Notch loss of function, Rme-8 is likely to have broader effects on endocytosis. In agreement, Wg distribution was also altered in *Rme-8*–depleted discs. Notably, Wg was detected at a broad range from its site of synthesis (Fig. 2 F) and accumulated within cells at a distance from the Wg-producing cells (Fig. S1 D). These consequences were similar to those reported for *Hrs* loss of function

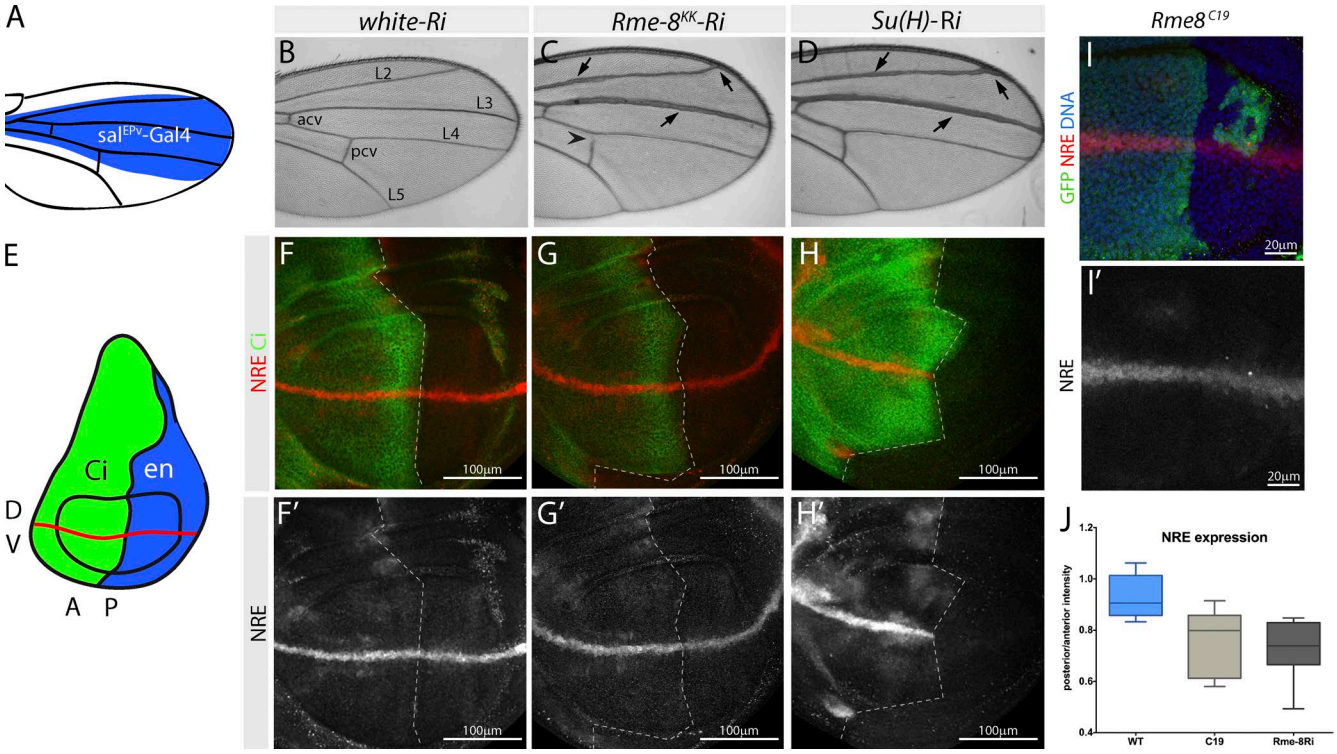

Figure 1. **Rme8 regulates Notch pathway function.** (A) *sal^{EPv}-Gal4* expression domain in an adult wing. (B–D) Adult wing from flies expressing *w* (B), *Rme-8* (C), or *Su(H)* (D) *Ri* with *sal^{EPv}-Gal4*. *Rme-8* knockdown results in vein thickening and small Dl's, similar to *Su(H)-Ri* treatment (arrows). Also note loss of posterior cross-vein (arrowhead; Pcv). L2–5 veins; Acv, anterior cross-vein. (E) *en-Gal4* expression domain in the posterior (P, blue) wing disc, as used in this and all subsequent knockdown experiments (F–H′) NRE-mCherry expression in wing discs from flies expressing *w* (F), *Rme-8* (G), or *Su(H)* (H) *Ri* (right of dashed line). *Rme-8-Ri* slightly reduced *NRE* expression, *Su(H)-Ri* causes loss of *NRE* expression. Cubitus interruptus (Ci) marks the unaffected anterior (A) compartment in this and all subsequent experiments. (I and I′) NRE-mCherry expression is decreased in *Rme-8* (*Rme-8^{c19}*) mutant cells (GFP negative). Mutant clones were generated using *FRT42D PCNA, Ubi-GFP; hh-flp*. (J) Box plot of anterior/posterior pixel intensity ratio, measured in comparable posterior and anterior regions of control, *Rme^{C19}* mutant (*C19; n = 7*), and *Rme-8* knockdown (*Rme-8Ri, n = 12*) discs. Boxes indicate 25th to 75th percentiles, whiskers represent maximum and minimum values in the dataset, and lines show the median values.

(Piddini et al., 2005; Rives et al., 2006) and suggest that Wg trafficking within receiving cells becomes compromised when *Rme-8* is depleted. In contrast, Wg secretion appeared relatively normal. First, the distribution of extracellular Wg in *Rme-8*–depleted tissue was similar to wild type (WT; Fig. S1 E). Second, *senseless*, a gene whose expression requires high levels of Wg signaling (Nolo et al., 2000) was still expressed in *Rme-8*–depleted cells (Fig. S1, F and G). These data argue that Wg secretion, which relies on retrograde recycling of its chaperone, Wntless, via a retromer-dependent route to the Golgi (Belenkaya et al., 2008; Franch-Marro et al., 2008; Pan et al., 2008; Port et al., 2008; Yang et al., 2008; Harterink et al., 2011; Zhang et al., 2011), was still functional in *Rme-8*–depleted cells, although other aspects of Wg trafficking were perturbed. As the adult phenotypes from *Rme-8* depletion are, however, most allied to deficits in Notch signaling, subsequent analysis was focused on the consequences on Notch trafficking and function.

Rme-8 regulates Notch trafficking

One strategy to investigate the stage at which trafficking is arrested is to follow the uptake of receptor-bound antibodies in live tissues (Le Borgne and Schweisguth, 2003). Using an antibody against NECD, we tracked the intracellular route by monitoring the location of antibody–Notch complexes at different times after the unbound antibody was washed out. First, we established mild conditions of *Rme-8* knockdown, so that, at time 0, there were similar levels of the α-NECD antibody bound at the cell surface in control and *Rme-8*–depleted compartments (Fig. 3, A, D, and I). We then transferred tissues to RT and analyzed changes in distribution.

After 30-min internalization, large amounts of the Notch–antibody complex were already accumulated in subapical puncta in *Rme-8*–depleted regions (Fig. 3, B, E, G, and H). After 2 h, these subapical puncta were more pronounced (Fig. 3, C′ and F–H), and the amount of Notch–antibody complex at the cell surface was reduced in comparison to neighboring WT tissue (Fig. 3, C and I). At this time, the internalized complexes in WT tissue were enriched basally (Fig. 3, C″ and F) and most likely corresponded to a prelysosomal compartment. The results therefore demonstrate that Notch is internalized in *Rme-8*–depleted tissue and accumulates in an apical compartment. In support, accumulation of Notch was prevented by combined knockdown of *Rme-8* with *avalanche* (Fig. S3 H), which is required at the earliest stages of endocytic trafficking (Lu and Bilder, 2005). The decrease in antibody-associated Notch at the membrane at 30 min and 2 h (Fig. 3 I) suggests either that Notch is endocytosed more rapidly in the absence of *Rme-8* or that there is a defect in recycling of Notch back to the plasma membrane after endocytosis. Given the previously observed association of Rme-8 with endosomes (Chang et al., 2004; Freeman et al., 2014), the latter seems more likely.

Notch trafficking is regulated by E3-ubiquitin ligases including Dx and Suppressor of Dx (Su(dx); Hori et al., 2004; Wilkin et al., 2004; Yamada et al., 2011). For example, over-

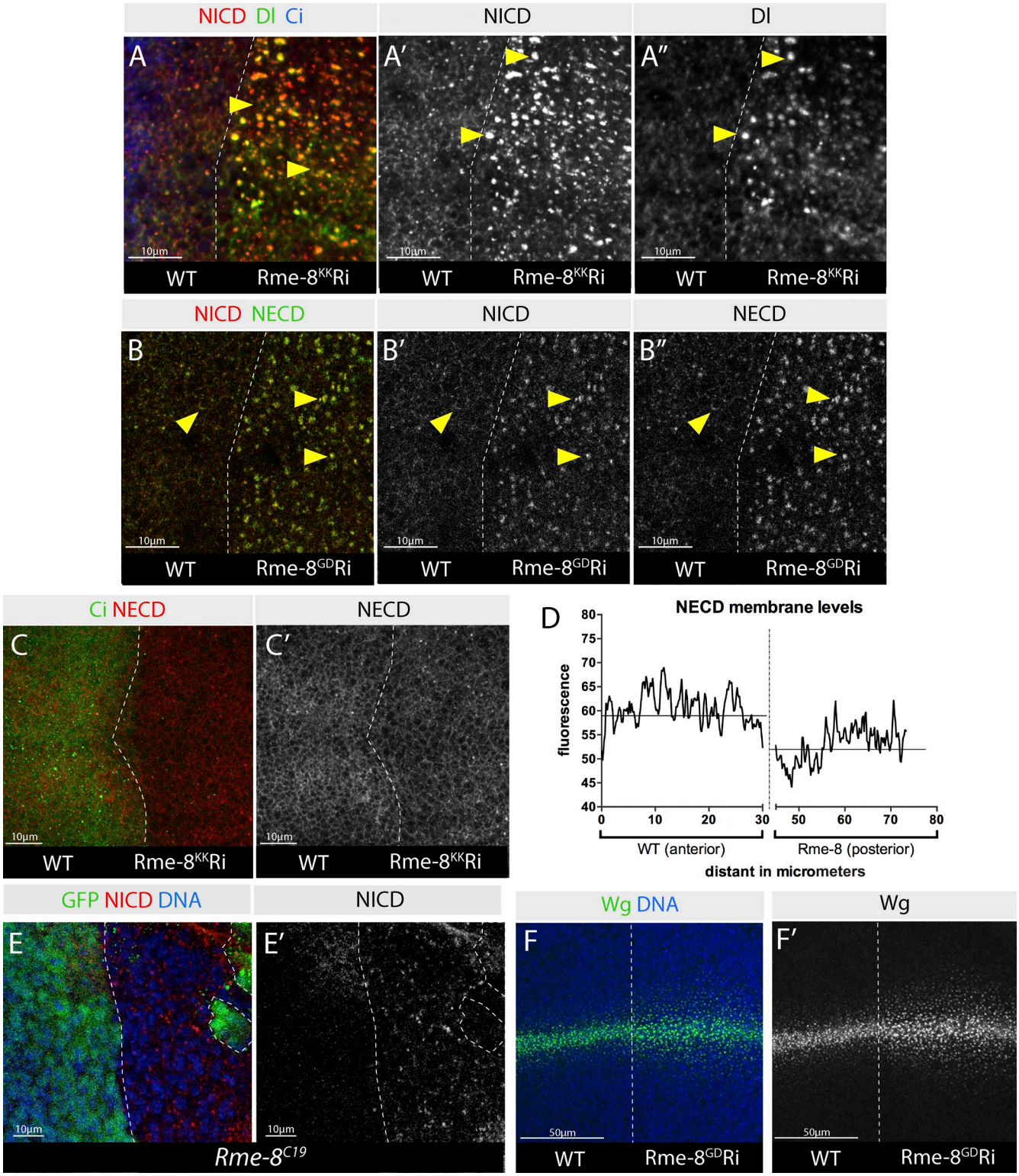

Figure 2. **Aberrant trafficking of Notch, Dl, and Wg in *Rme-8*–depleted cells.** (A–B″) Effects of *Rme-8 Ri* on Notch (anti-NICD, red in A and B; anti-NECD, green in B) and Dl (green in A) trafficking. Both, full-length Notch and Dl accumulate together inside *Rme-8-Ri* cells (arrowheads). Depleted territory in this and subsequent figures is on the right side of dashed line, unless stated otherwise. (C and C′) NECD (staining without detergent) is depleted from the membrane when *Rme-8* is knocked down (*Rme-8*^{KK}). (D) Quantification of surface NECD levels from C. The data shown are from a single representative disc; $n = 6$ for the experiment shown; the experiment was repeated three times with similar results. Line shows mean fluorescence at the membrane level within the specified compartment. (E and E′) Intracellular Notch puncta accumulate in *Rme-8*^{C19} mutant cells (GFP negative, marked by dashed line; generated as in Fig 1 I). (F and F′) Wg is detected more broadly in the *Rme-8-Ri* tissue.

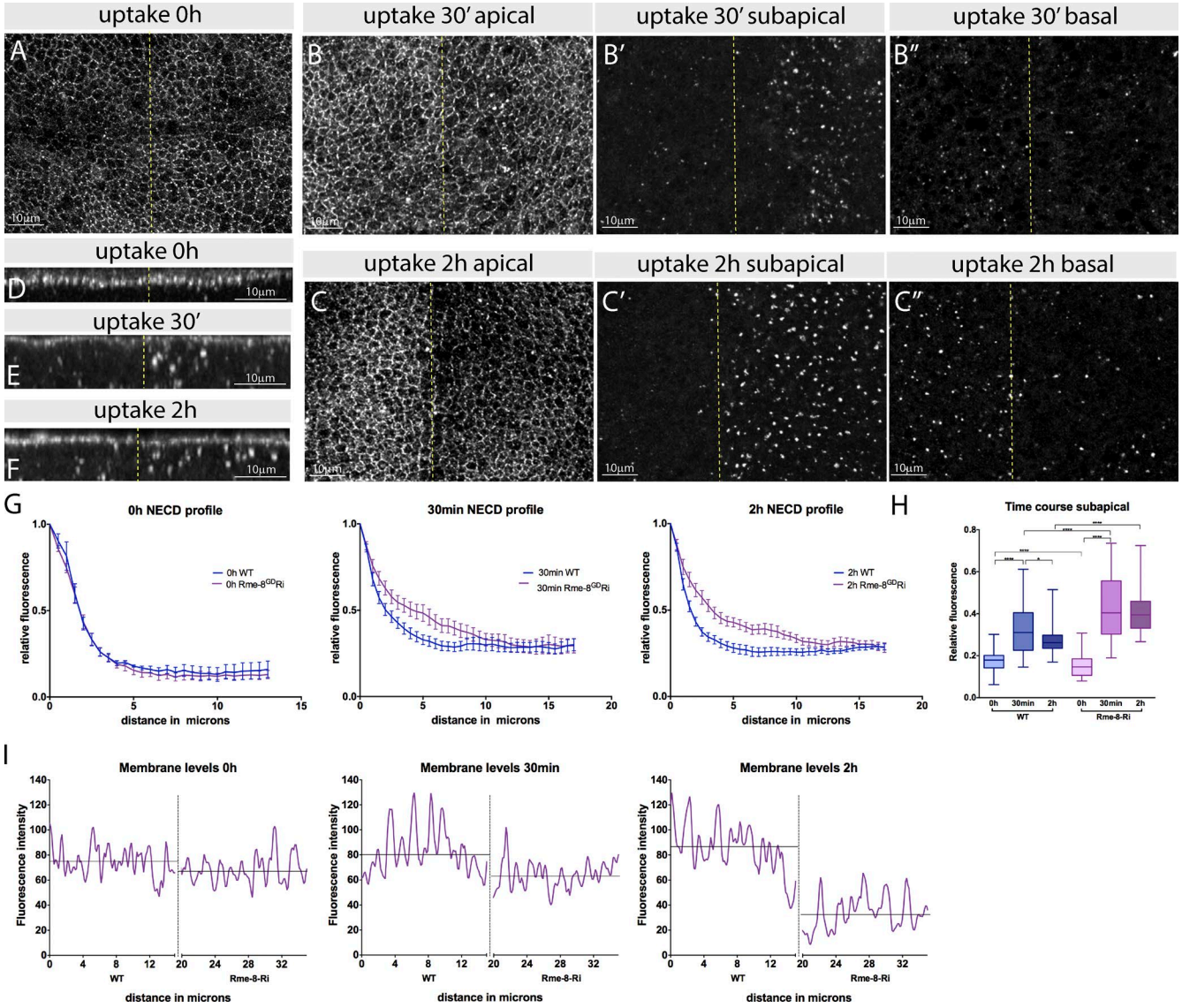

Figure 3. **Notch accumulates in subapical puncta in Rme-8–depleted cells.** (A–C″) Antibody uptake assay to detect Notch trafficking (anti-NECD) in cultured wing discs. Different focal planes (apical [A, B, and C]; subapical [B′ and C′]; basal [B″ and C″]) from xy sections at 0 min (A), 30 min (B), or 2 h (C) after uptake. (D–F) xz cross sections of discs in A, B, and C, respectively. Notch–antibody complexes accumulate subapically in *Rme-8-Ri* (right) after 30 min but accumulate more basally in WT (left). (G) Quantification of fluorescence levels from Notch–antibody complexes according to distance from apical membrane in xz cross sections (apical levels were normalized to 1 for comparisons between samples). At 30 min and 2 h, more anti-NECD is detected in subapical regions with *Rme-8-Ri* compared with WT. Error bars represent the SEM. (H) Comparison between subapical levels of anti-NECD detected at different time points in wild-type (WT) and *Rme-8 Ri* tissue. Boxes indicate 25th to 75th percentiles, whiskers represent maximum and minimum values in the dataset, and lines show the median values. Asterisks indicate significance according to a one-way analysis of variance test; *, P = 0.05–0.01; ****, P < 0.0001. (I) Quantification of apical membrane anti-NECD in anterior (left, WT) versus posterior (right, *Rme-8 Ri*) of discs in A–C. The data shown are from a single representative disc; *n* = 10 for the experiment shown; the experiment was repeated two times with similar results. Lines show mean fluorescence at the membrane level within the specified compartment.

expression of Dx modifies the destination of Notch, causing ectopic activation detectable by ectopic NRE-GFP expression and tissue overgrowth (Fig. S2 A; Hori et al., 2004; Yamada et al., 2011). However, neither ectopic Notch activation nor overgrowth phenotypes were reduced when *Rme-8* was depleted in Dx-overexpressing discs (Fig. S2 B), suggesting that they operate on different trafficking routes. In addition, Notch accumulations were detected throughout the cell, not just subapically as in *Rme-8* knockdown (Fig. S2, C–F). In converse experiments, Dx knockdown led to membrane accumulation of Notch, whereas the phenotype in combination with *Rme-8-Ri* appeared to be an aggregate (Fig. S2, G–L). Likewise, similar experiments combining *Rme-8-Ri* with Su(dx) overexpression also yielded an aggregate of phenotypes (Fig. S2, M–P). Together, these results suggest that the pools of Notch modified by Dx and Su(dx) are likely to be separate from those trapped by *Rme-8* knockdown.

Rme-8 depletion results in enlarged endosomes, where Notch accumulates in proximity to Rab4, and alters Notch dynamics at the membrane

To investigate where in the endocytic network Notch accumulated when *Rme-8* was depleted, tissues were co-stained for Notch and endosomal markers (summarized in Fig. S3, G and

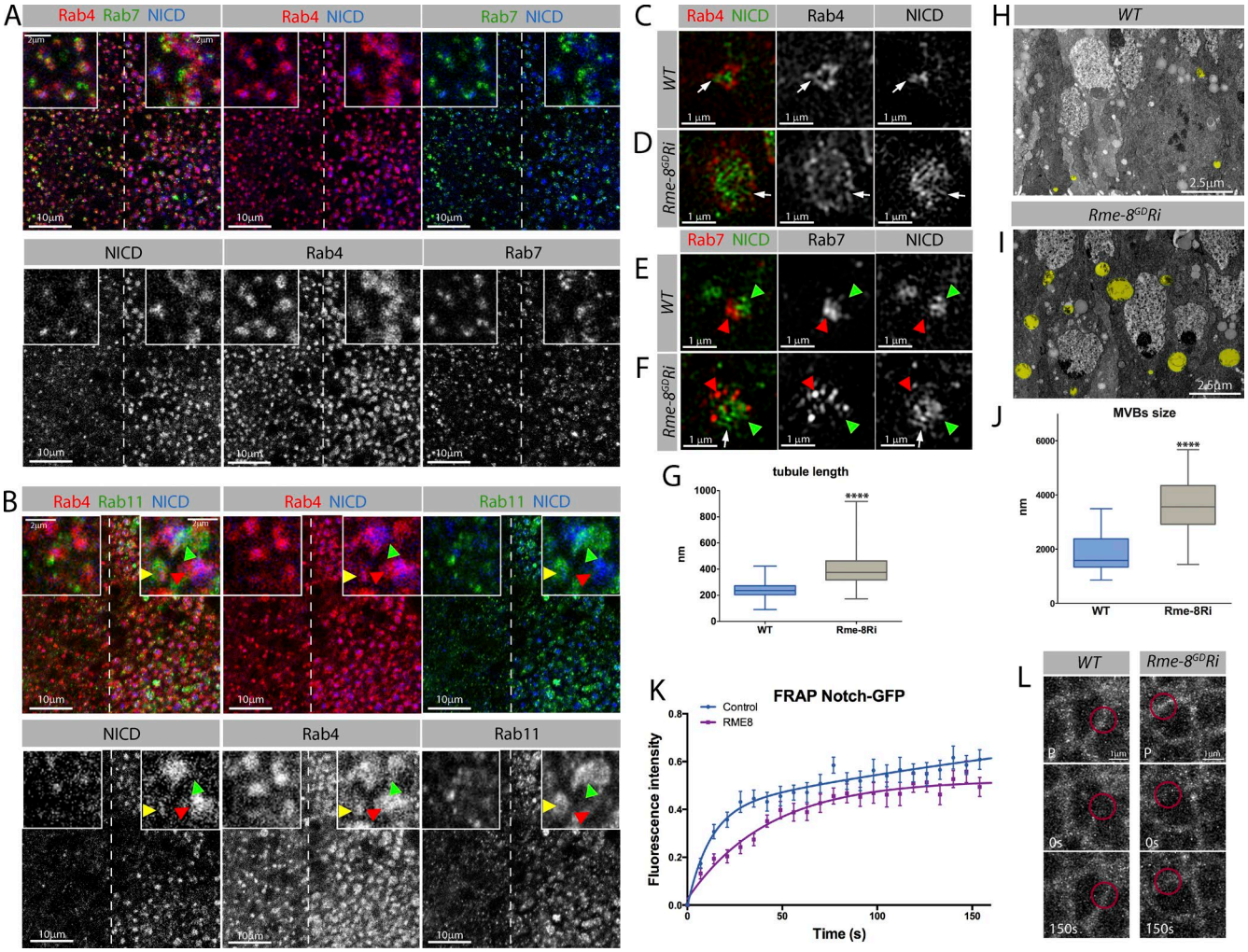

Figure 4. **Notch associates with enlarged endosomes and recovers more slowly at the membrane in *Rme-8*–depleted cells.** (A) Enlarged puncta containing NICD, Rab4, and Rab7 are detected in *Rme8-Ri*, where NICD accumulates in proximity to Rab4 (see insets). (B) Enlarged puncta containing NICD, Rab4, and Rab11 were detected in *Rme-8-Ri* cells. Some puncta contain all three proteins (insets, yellow arrowheads), others contain Rab11 only (insets, green arrowheads) or Rab4+NICD (insets, red arrowheads). (C–F) Superresolution images of endosomes from WT (C and E) or *Rme-8*-Ri (D and F) wing disc cells stained for NICD and Rab4 (C and D) or Rab7 (E and F). Notch localizes adjacent to Rab4 in protrusions (arrows, C). In *Rme-8*–depleted cells, tubule-like protrusions appear more extensive (arrows, D). Rab7 labels a compartment adjacent to NICD accumulations, both in WT and *Rme-8-Ri* cells (arrowheads, E and F). (G) Measurements of protruding Rab4-labeled tubule-like structures on endosomes from WT and *Rme-8* knockdown (≥50 tubules/disc; 5 discs per genotype). Asterisks indicate significance according to Mann–Whitney test: ****, $P < 0.0001$. (H and I) Sections from WT (H) or *Rme-8-Ri* (I) regions of a wing disc analyzed by TEM, with endosomes highlighted in yellow. (J) Quantification of endosome perimeters from TEM images. (WT $n = 28$; *Rme-8-i+w-Ri* $n = 76$.) Asterisks indicate significance according to *t* test; ****, $P < 0.0001$. (K and L) FRAP experiments, measuring recovery of Notch-GFP after photobleaching. (K) Plot of averaged recovery curves (mean ± SEM) with best-fit curves as solid lines. Boxes indicate 25th to 75th percentiles, whiskers represent maximum and minimum values in the dataset, and lines show the median values. (L) Single FRAP examples with red circles showing bleach spots. (P, prebleach). The recovery curves could be described by a biexponential equation (WT, $P < 0.0001$; Rme-8, $P = 0.02$; Bulgakova et al., 2013; see Materials and methods) suggestive of two recovery processes, fast diffusion within the membrane and slower endocytic trafficking. Both appear affected by Rme-8 depletion.

K). First, Rab5 puncta showed little change in *Rme-8*–deficient cells, indicating that early endosomes form normally, and relatively few Rab5 puncta were associated with Notch (Fig. S3 A). Second, markers of maturing endosomes, Rab7 and Hrs, were present in larger aggregates than in WT (Fig. 4 A and Fig. S3 B) that were found in proximity to large Notch accumulations, although there was limited colocalization. Third, Notch puncta were also labeled by the phosphatidylinositol 3-phosphate sensor FYVE-GFP and by the FYVE domain–containing protein SARA (Smad anchor for receptor activation), indicating that Rab5-mediated recruitment of phosphatidylinositol-3-kinase had occurred (Fig. S3, C and E). The size of SARA puncta was also increased. Finally, the endolysosomal protein, Lamp1, was detected in enlarged structures, although showed relatively low colocalization with Notch (Fig. S3 F). These results indicate that loss of *Rme-8* affects maturing endosomes and that, although Notch is associated with these, it is primarily confined to a domain distinct from those marked by Hrs or Rab7 (Fig. S3 K).

Other endosomal subdomains include those involved in Rab4- and Rab11-dependent recycling to the plasma membrane (Sönnichsen et al., 2000; Li et al., 2008; Grant and Donaldson, 2009). As with other markers, *Rme-8* depletion resulted in enlarged Rab4 and Rab11 puncta, which largely segregated into distinct domains (Fig. 4 B). The most marked effect was with Rab4, which also exhibited the most intimate relationship with Notch (Fig. 4, A and B). The retromer Vps26 subunit showed a

similar colocalization (Fig. S3 D). Altogether, the results support a model in which the absence of *Rme-8* generates maturing endosomes that are comprised of an array of enlarged subdomains. The preferential relationship between Notch, Rab4, and Vps26 in this enlarged structure suggests that the receptor is trapped in a recycling compartment (Fig. S3 K).

Using 3D structured illumination microscopy, it was possible to further resolve the endosomal structures containing Notch. In WT cells, Notch associated with Rab4-labeled endosomal structures with a perimeter of ∼2.5–3.5 µm (Fig. 4 C). Elongated Rab4- and/or Notch-labeled structures extended out from and across each endosome, consistent with them forming part of the tubular endosomal network (e.g., Fig. 4 C, arrows). Punctate Rab7 was normally segregated into an adjacent domain, although occasionally Rab7 and Notch puncta were directly juxtaposed (Fig. 4 E, arrowheads). After *Rme-8* depletion, Notch and Rab4 were present in enlarged structures ∼4–6 µm in perimeter (Fig. 4 D). A punctuated circumferential ring of Rab4 was usually evident but was larger in *Rme-8*–depleted tissues, and the protrusions, likely tubules, were more extensive (Fig. 4, D and G). Alternating segments of Rab4 and Notch were detected in several of these, suggesting they are present in the same protrusions (Fig. 4 D, arrows). Rab7 was also associated with the same large structures but was largely segregated from Notch (Fig. 4 F, arrowheads). Altogether, these results indicate that Notch accumulates preferentially in Rab4 positive compartments and show that the endosomes detected after *Rme-8* depletion are enlarged with more extensive tubule-like structures than in WT. A similar increase in highly branched endosomal tubules occurred in *Rme-8*–depleted HeLa cells (Freeman et al., 2014).

Enlarged maturing endosomes were also detected by transmission EM (TEM; Fig. 4, H–J; and Fig. S4). Sectioning the discs to directly compare WT and *Rme-8*–depleted tissue showed that the mean size of MVBs (identified by the presence of ILVs) was 2–3× greater than in WT (Fig. 4 J and Fig. S4, D, H, and I). Although the TEM did not capture the tubular morphology suggested by the superresolution images, the size of the structures observed was similar using the two methods (2.5–4-µm perimeter). Thus, it appears that in the absence of *Rme-8*, the vacuolar endosome and associated tubular network become greatly enlarged.

The localization experiments show that a significant proportion of Notch associates with Rab4 when *Rme-8* is reduced. One explanation is that Rme-8 is necessary for normal recycling of Notch and that, when Rme-8 is missing, Notch is trapped in a recycling domain of the sorting endosome. To investigate further, we monitored the dynamics of Notch protein at the membrane via FRAP (Fig. 4, K and L) using a functional Notch-GFP fusion protein (Couturier et al., 2012). Small circular regions along apical cellular junctions were bleached, (Fig. 4 L, red circles) and the reappearance of unbleached Notch-GFP was measured in WT and *Rme-8*–depleted cells. The recovery with time was significantly altered in *Rme-8*–depleted cells compared with WT controls (Fig. 4 K). These data demonstrate that the dynamics of Notch proteins at the membrane are reduced. Furthermore, the Notch-GFP recovery was also curtailed by treating the tissues with the dynamin inhibitor dynasore, indicating that endocytic trafficking contributes to the recovery (Fig. S3, I and J). However, these results do not unequivocally demonstrate that recycling is affected in the Rme-8–depleted cells, as several factors can contribute to recovery and the experiments are not able to distinguish direct from indirect effects. Nevertheless, as Notch becomes trapped with Rab4 and Vps26 in the Rme-8–depleted cells, it is likely that the reduced recovery of Notch-GFP reflects, in part, a defect in endocytosis-mediated recycling

Combined knockdown of Vps26 and Rme-8 leads to ectopic Notch activity

Many recycling pathways involve the retromer complex, including the Rab4-associated route to the plasma membrane (Temkin et al., 2011; Seaman, 2012; Seaman et al., 2013; Steinberg et al., 2013; Wang et al., 2014). Furthermore, *Rme-8* localizes at places where retromer-mediated sorting occurs (Popoff et al., 2009; Shi et al., 2009; Freeman et al., 2014). To investigate whether Notch trafficking defects in *Rme-8*–depleted cells involve retromer, we analyzed the consequences from depleting *Vps26*.

First, we monitored consequences on *NRE-mCherry* when *Vps26* was depleted either alone or together with *Rme-8*. *Vps26* single knockdown had little impact on NRE-mCherry expression (Fig. 5 A), indicating that Notch activity was not substantially changed by retromer depletion as reported previously (Franch-Marro et al., 2008). Strikingly, however, the combined knockdown of *Vps26+Rme-8* resulted in NRE expression throughout the domain, indicating that this combination results in strong ectopic Notch activation (Fig. 5 B). The reduced Vps26 protein levels (Fig. S5 A) along with the accumulation of Wg (Fig. 5 C), whose secretion depends on retrograde transport of Wntless in a retromer-dependent manner, confirmed the efficacy of *Vps26* knockdown (Belenkaya et al., 2008; Franch-Marro et al., 2008; Pan et al., 2008; Port et al., 2008; Yang et al., 2008; Harterink et al., 2011; Zhang et al., 2011). The slight broadening of Wg expression in *Vps26+Rme-8* combined knockdowns is consistent with the ectopic *NRE-mCherry* expression in this genotype (Fig. 5 D) because *wg* is a Notch target. Mutations affecting a second component of the retromer complex, Vps35, had a similar effect to Vps26 *Ri*. Thus, *Rme-8* knockdown in *Vps35* mutant cells resulted in ectopic expression of *deadpan*, a HES (Hairy and Enhancer of split) gene directly regulated by Notch in this tissue (Fig. S5, B–D).

In agreement with the minimal effects on *NRE-mCherry* expression, there was little consequence on Notch intracellular distribution or Notch membrane levels after depletion of *Vps26* alone (Fig. 5, E and F). However, membrane Notch levels were reduced in *Vps35* mutant cells, suggesting that retromer does contribute to Notch trafficking (Fig. S5 E). In addition, V*ps26* depletion had pronounced effects in the context of reduced *Rme-8* (Fig. 5, G and H). The enlarged Notch puncta, characteristic of *Rme-8* depletion, were absent in the combined *Rme-8; Vps26* knockdown (Fig. 5 H). The levels of apical, membrane-associated, Notch were also very strongly reduced in this condition (Fig. 5 G). Moreover, the Rab7 puncta localized more basally, although they were still slightly enlarged compared with WT (Fig. 5 H″). Finally, the TEM suggests that the *Vps26* depletion partially suppressed the MVB enlargement caused by loss of *Rme-8* (Fig. 5, I and J; and Fig. S4, G–I).

In the absence of *Vps26* and *Rme-8*, it appears that Notch is neither recycled to the membrane nor trapped in enlarged endosomes. This fits with the cargo-sorting role of *Vps26* and suggests that, in its absence, Notch fails to become concentrated into a retromer-dependent recycling domain. Instead, Notch must be redirected into other endosomal routes, possibly the endolysosomal pathway where ectopic activation can occur if Notch remains in the limiting membrane (Wilkin et al., 2004, 2008; Hori et al., 2011).

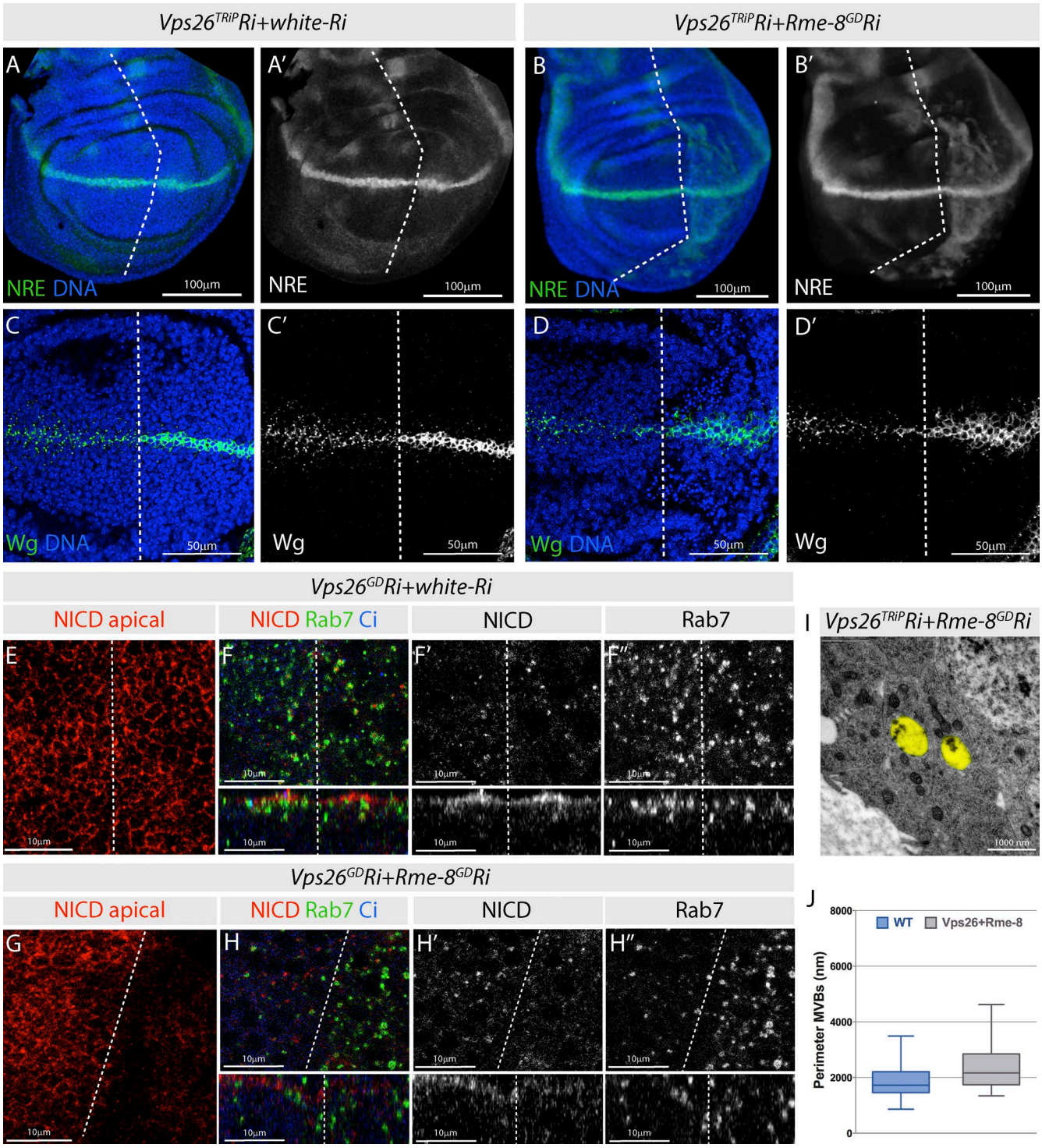

Figure 5. **Combined depletion of *Rme-8* with *Vps-26* results in ectopic Notch activation.** (A–B′) NRE-mCherry is ectopically expressed in *Vps26-Ri;Rme8-Ri* (B) compared with *Vps26-Ri;w-Ri* (A). (C–D′) Wg accumulates inside both producing and receiving cells in *Vps26-Ri;Rme8-Ri* (D) but only in producing cells in *Vps26-Ri;w-Ri* (C). (E–H″) NICD and Rab7 distribution in *Vps26-Ri;w-Ri* (E and F) or *Vps26-Ri;Rme-8-Ri* (G and H) wing discs. Apical (E and G) and subapical focal planes (F and H) with xz cross sections from discs in F and H beneath. (I and J) TEM images of *Vps26-Ri;Rme8-Ri* (I) with endosomes colored in yellow, and quantification of endosomal perimeter from TEM images (J; WT $n = 83$; Vps26-Ri+Rme-8-Ri $n = 30$). Boxes indicate 25th to 75th percentiles, whiskers represent maximum and minimum values in the dataset, and lines show the median values.

Removal of ESCRT-0 components in combination with Rme-8 results in ectopic Notch activation and hyperplasic growth

Proteins destined for lysosomal degradation become segregated into ILVs through the activity of four ESCRT complexes (Hurley and Emr, 2006). The first, the ESCRT-0 complex containing Hrs (hepatocyte growth factor–regulated tyrosine kinase substrate) and Stam (signal transducing adaptor molecule), sorts ubiquitinylated cargoes destined for ILVs into clathrin-coated patches. In addition, Hrs has been suggested to act antagonisti-

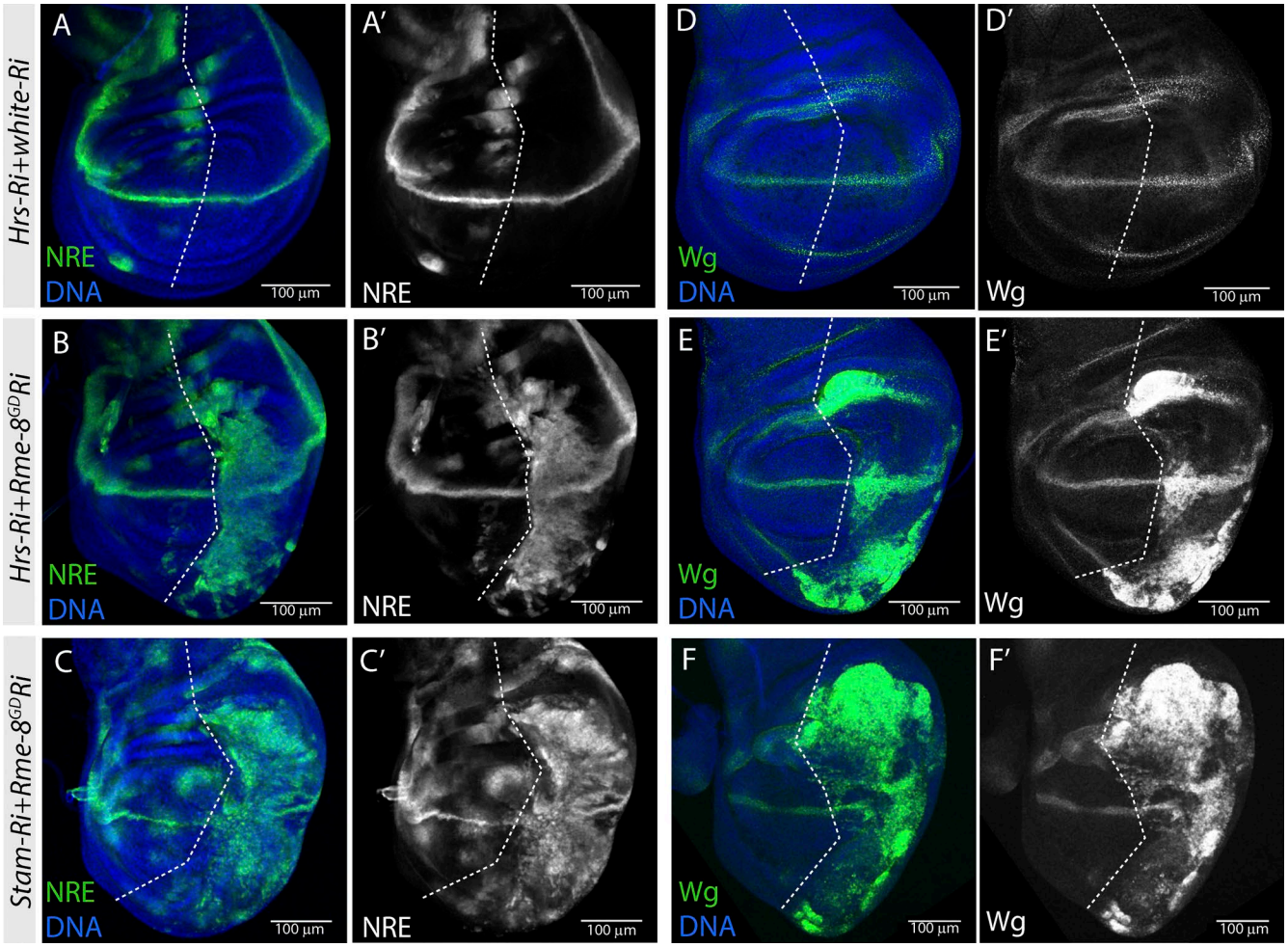

Figure 6. **Combined depletion of *Rme-8* with *ESCRT-0* results in ectopic Notch activation and tissue overgrowth.** (A–F′) NRE-GFP (A–C) and Wg (D–F) expression are strongly up-regulated in *Hrs+Rme-8* double knockdown (B and E) and *Stam+Rme8* double knockdown (C and F), in contrast to the *Hrs* single knockdown where expression is unaffected (A and D, *Hrs-Ri;w-Ri*).

cally toward complexes containing *Rme-8* and retromer to coordinate sorting functions on early endosomes (Popoff et al., 2009). We therefore analyzed the consequences when *Hrs* or *Stam* were depleted in combination with *Rme-8*.

First, we tested effects on *NRE-GFP* expression. As reported (Vaccari et al., 2008), this showed little change after knockdown of either ESCRT-0 (Fig. 6 A). Surprisingly, when either *Hrs* or *Stam* were depleted together with *Rme-8*, *NRE* expression was strongly up-regulated, indicative of extensive ectopic Notch activation (Fig. 6, B and C). This was even greater than that seen with the *Vps26* combination and was accompanied by concomitant tissue overgrowth, similar to the hyperplasia observed when other endocytic regulators were compromised (Moberg et al., 2005; Thompson et al., 2005; Vaccari and Bilder, 2005; Childress et al., 2006; Morrison et al., 2008; Vaccari et al., 2008, 2009). In general, the effects were stronger in the *Stam;Rme-8* combination than in *Hrs;Rme-8* (Fig. 6, B and C), possibly reflecting differences in depletion efficiencies for *Stam* and *Hrs Ri* lines, although the latter was nevertheless sufficient to cause substantial reduction in Hrs protein levels (Fig. S5 F).

The outcome on *wg* expression was similar to that on NRE. In *Hrs* or *Stam* single knockdown, more Wg accumulated inside receiving cells, suggesting that steady-state levels are affected by the amount of protein routed to lysosomes. However, there was no expansion of the expression domain (Fig. 6 D). In contrast, when *Rme-8* was depleted together with *Hrs* or *Stam*, there was widespread ectopic expression of Wg, similar to NRE (Fig. 6, E and F). Finally, ectopic *NRE-GFP* expression was also seen when *Rme-8 Ri* was expressed in *Hrs* mutant clones (Fig. S5 G). Thus, the removal of *Rme-8* uncovers a profound requirement for ESCRT-0 to prevent ectopic Notch activation, which is not evident under normal conditions.

Several studies show that ectopic activation can occur when Notch is trapped at the limiting membrane of mature endosomes marked by Rab7 (Wilkin et al., 2004, 2008; Hori et al., 2011; Schneider et al., 2013). As reported previously, in cells depleted for *Hrs* alone, Notch accumulated in large Rab7 puncta (Fig. 7, A and F). When *Hrs* and *Rme-8* were knocked down simultaneously, Notch puncta size increased (Fig. 7 B), and larger Notch-stained structures were detected by superresolution microscopy (Fig. 7 F). However, the Notch-enriched regions in the combined *Hrs;Rme-8* knockdown were not more coincident with Rab7 (Fig. 7 B) than in the WT or *Hrs*-depleted tissue (Fig. 4, A and E; and Fig. 7 A), and the superresolution images from *Hrs;Rme8* tissues did not reveal any increase in overlap between Rab7 and the large Notch conglomerates. Indeed, Rab7 was frequently present in dispersed clusters of dif-

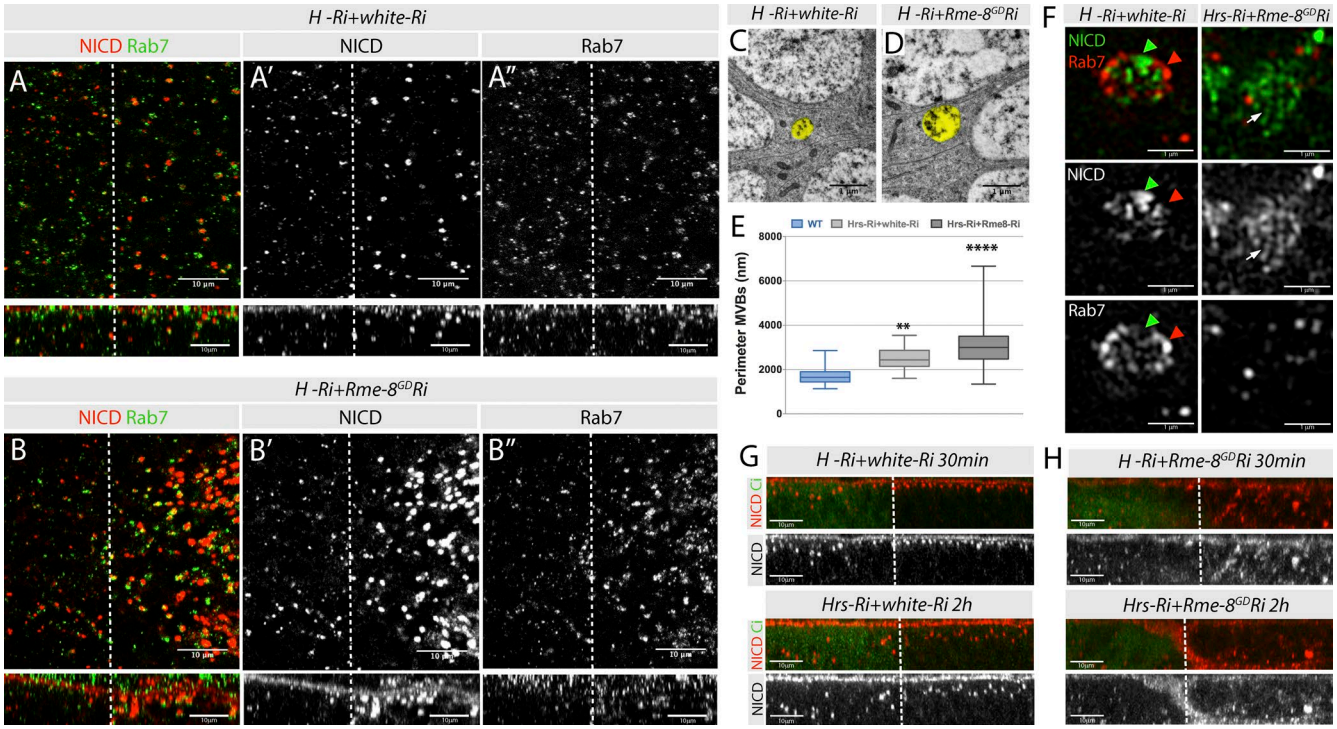

Figure 7. **Effects on Notch trafficking of combined *Rme-8* and *ESCRT-0* depletion.** (A–B″) Distribution of NICD and Rab7. xy section of discs at the subapical plane (top) and xz cross sections of the same specimens (bottom). Notch accumulates in enlarged Rab7 structures upon *Hrs* knockdown (A; *Hrs-Ri+w-Ri*) but not in double knockdown (B; *Hrs-Ri+Rme8-Ri*). (C and D) TEM images of *Hrs-Ri;w-Ri* (C) or *Hrs-Ri;Rme8-Ri* (D) with endosomes colored in yellow. (E) Quantification of endosome perimeters from TEM images (WT $n = 83$, *Hrs-Ri+w-Ri* $n = 33$, and *Hrs-Ri+Rme-8Ri* $n = 42$). Boxes indicate 25th to 75th percentiles, whiskers represent maximum and minimum values in the dataset, and lines show the median values. Asterisks indicate significance according to one-way analysis of variance test; **, P = 0.01–0.001; ****, P < 0.0001. (F) Superresolution images of single endosomes from *Hrs-Ri;w-Ri* (left)– or *Hrs-Ri;Rme8-Ri* (right)–expressing discs, stained for NICD and Rab7, which appear to localize in the same vesicular compartment in *Hrs* knockdown (arrowheads, left), but not in the *Rme-8-Hrs* double knockdown, where Notchlocalizes in long tubules (arrows, right). (G and H) Antibody uptake assay for Notch in cultured wing imaginal discs expressing *Hrs-Ri;w-Ri* (G) or *Hrs-Ri;Rme8-Ri* (H).

fuse small puncta (Fig. 7 F). Finally, the MVBs detected by TEM in this combination were larger than with *Hrs* knockdown alone (Fig. 7, C–E), but the mean perimeter was not significantly different from *Rme-8-Ri* alone (Fig. S4), suggesting that the MVB is not further enlarged in the double combination. One possibility is that, although the vacuolar endosome/MVB is not enlarged, the Notch tubulated region is more extensive in *Hrs-Ri+Rme-8-Ri* than in *Rme-8-Ri* alone, as suggested by the size of the Notch-stained structures in the superresolution images (Fig. 7 F, arrows).

One difference between the Notch accumulations detected in *Hrs* alone compared with the combined knockdown was their apical–basal position as detected in uptake assays. In *Hrs* knockdown, internalized Notch remained trapped close to the apical surface, even after 2 h (Fig. 7 G). In contrast, when both *Hrs* and *Rme-8* were perturbed, large Notch accumulations were present in basal regions (Fig. 7 H). This result suggests that, when both Hrs and Rme-8 are reduced, Notch becomes trapped at a later stage in the endosomal pathway. In addition, more Notch accumulated than in either single knockdown, consistent with multiple different trafficking routes being perturbed by this combination.

Ectopic Notch activation in the *Rme-8* combinations is not dependent on Kuzbanian (Kuz)

In many instances in which Notch becomes activated in the endocytic network, it does not require ligands (Hori et al., 2004; Thompson et al., 2005; Childress et al., 2006; Jaekel and Klein, 2006; Vaccari et al., 2008). To assess whether this might the case in the combinations with *Rme-8*, we tested whether activation could be prevented by expression of dominant-negative ADAM 10/*kuz*, the protease mediating the ligand-dependent S2 cleavage of Notch. Expression of Kuz^{DN} in either *Vps26;Rme-8* or *ESCRT-0;Rme-8* double knockdown was not able to suppress ectopic *NRE* expression (nor ectopic expression of another Notch target, *deadpan*) although it blocked the normal D/V expression of *NRE* (Fig. 8, A–D). Moreover, expression of Kuz^{DN} alone prevented D/V boundary expression of *wg*, in which it is dependent on Notch activity, without affecting hinge expression hinge, where it is Notch independent (Fig. 8 E). The former confirmed that Kuz^{DN} was effectively inhibiting ligand dependent signaling, suggesting that the residual NRE expression when kuz^{DN} is combined with *Vps26;Rme-8* or *ESCRT-0;Rme-8* arises through ligand-independent activation. However, expression of Kuz^{DN} did rescue the overgrowth produced by depletion of *ESCRT-0* and *Rme-8* (Fig. 8, F–H). One possible explanation is the positive feedback loop that occurs in this tissue, whereby expression of ligands is positively up-regulated in response to Notch activation (de Celis and Bray, 1997). Hence, any ligand-independent activity might be amplified by subsequent induction of ligand expression. Inhibiting Kuz function would prevent this amplification, limiting the ectopic Notch activity and tissue overgrowth to that from the ligand-independent route. Alternatively, Kuz might affect another growth regulatory pathway independent of Notch. Despite these secondary effects,

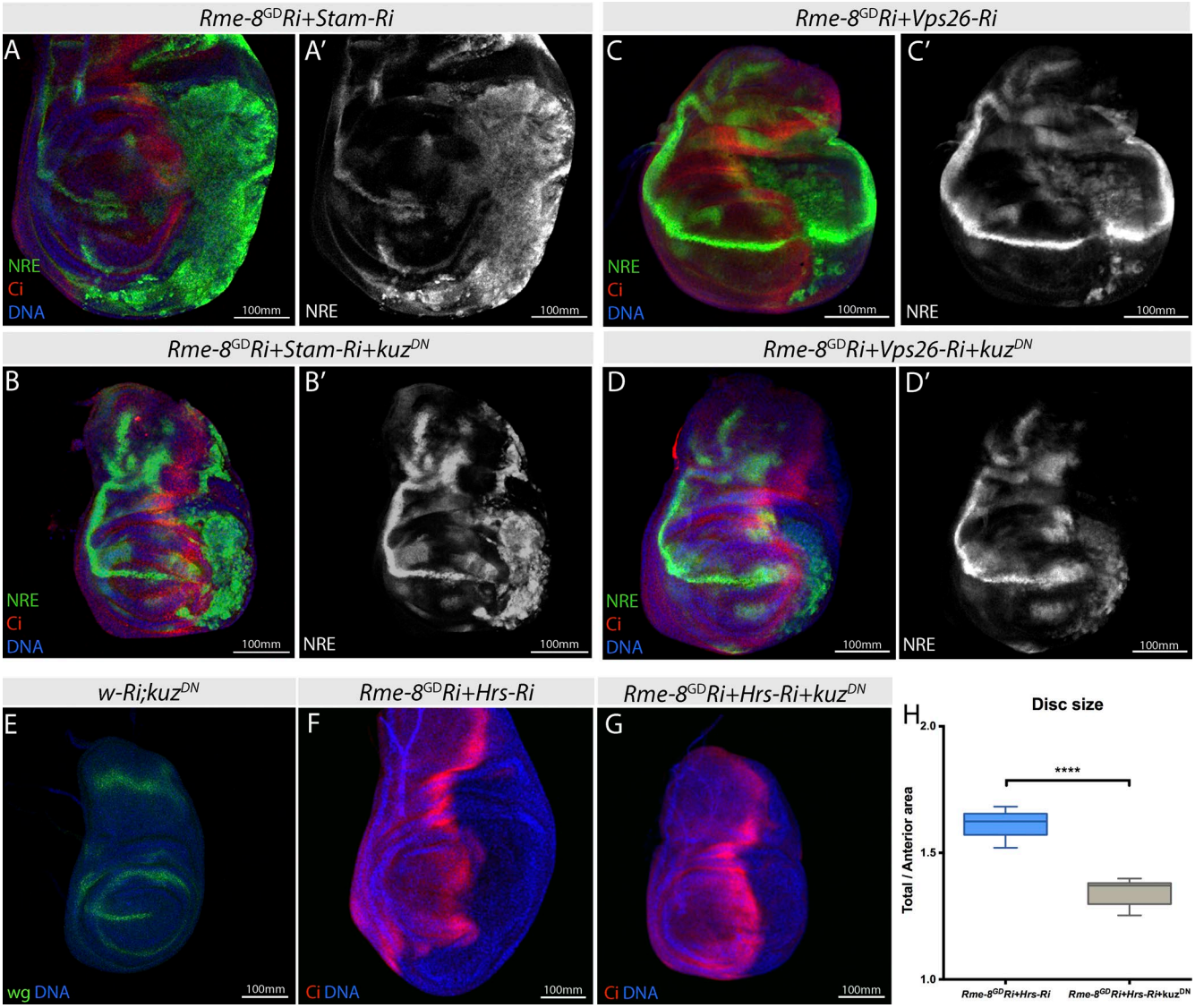

Figure 8. **Ectopic Notch activation observed in combined depletions is not prevented by Kuz^{DN}.** (A–D′) NRE-GFP expression shows that ectopic Notch activation in *StamRi+Rme-8-Ri* (A) or *Vps26-Ri+Rme-8-Ri* (C) is not rescued by *kuz*^{DN} coexpression (B and D). (E) Wg D/V expression is lost in discs expressing *kuz*^{DN} alone. (F and G) *kuz*^{DN} coexpression rescues overgrowth caused by *Hrs-Ri+Rme-8-Ri*. (H) Quantification of wing disc size for genotypes shown in F and G. Boxes indicate 25th to 75th percentiles, whiskers represent maximum and minimum values in the dataset, and lines show the median values. Asterisks indicate significance according to *t* test; ****, $P < 0.0001$.

it is evident that a significant proportion of ectopic Notch activation remained in the presence of Kuz^{DN}, suggesting it arose via a ligand-independent mechanism.

Discussion

Cells continuously internalize Notch, where much of it is routed to lysosomes for degradation. This process must be carefully regulated, not only to ensure steady-state levels of surface expression but also to prevent inappropriate activation within the endosomal pathway (Moberg et al., 2005; Thompson et al., 2005; Vaccari and Bilder, 2005; Childress et al., 2006; Morrison et al., 2008; Vaccari et al., 2008, 2009). Our analysis of *Rme-8* function reveals the importance of another aspect of trafficking, endocytic recycling, in maintaining sufficient levels of Notch at the membrane for signaling to occur correctly. As previous studies have not detected any requirement for retromer in normal Notch pathway function (Belenkaya et al., 2008; Franch-Marro et al., 2008; Pocha et al., 2011), we were surprised to find that Notch pathway activity was sensitive to depletion of *Rme-8*. In addition, the consequences from combined knockdown of *Rme-8* with *Hrs*, *Stam*, or *Vps26* show that Rme-8 is important to prevent inappropriate Notch activation when these cargo-sorting complexes are disrupted. Combined knockdowns resulted in high levels of ectopic Notch signaling and tissue hyperplasia, which could be of significance in the context of recently identified disease-linked mutations in *Rme-8* and other retromer members (Vilariño-Güell et al., 2011, 2014; Zimprich et al., 2011; McGough et al., 2014; Miura et al., 2014; Zavodszky et al., 2014).

In *Rme-8*–deficient tissues, Notch accumulated with Rab4 in enlarged endosomal structures and was depleted from the cell surface. Structured illumination microscopy suggested that

it was trapped in Rab4-positive tubular structures, which have not previously been detected in *Drosophila*, although tubular Rab5 plasma membrane invaginations have been observed (Fabrowski et al., 2013). FRAP measurements were compatible with the hypothesis that Notch recycling was compromised under these conditions, making it likely that Rme-8 is necessary for Rab4-mediated recycling and that recycling is important to maintain membrane Notch levels. Notably, however, signaling was only detectably impeded when apical levels of Notch were significantly compromised. This is surprising given that Notch activity is dosage sensitive. One possible explanation is that signaling depends critically on the relative levels of Notch and Dl (de Celis and Bray, 1997; Sprinzak et al., 2010) and that, because trafficking of both proteins was perturbed in the *Rme-8* knockdown, the impact may have been lessened. Another possibility is that the Notch pool engaged in functional signaling is localized away from the apical surface, where it is protected from defects in apical recycling. For example, some studies have suggested that signaling occurs between basal filopodia (de Joussineau et al., 2003; Cohen et al., 2010) and others have indicated that different receptor pools exist depending on modification state and/or presence of adaptors (Wilkin et al., 2008).

Notch accumulation in *Rme-8*–depleted tissue appeared strictly dependent on Vps26, a key component of sorting retromer, whereas reducing the latter alone had only minor effects on membrane Notch levels. This raises the possibility that another recycling pathway requiring Rme-8 can partially compensate, via the activity of other sorting complexes. One candidate for such alternative sorting could be Hrs, which appears to be involved in sorting cargoes for a fast recycling route as part of the CART complex (actinin-4, Brain-Expressed RING finger protein, myosinV; Hanyaloglu et al., 2005; Yan et al., 2005; Millman et al., 2008). Conversely, the Snx3-retromer–dependent pathway, which recycles Wntless to the Golgi (Harterink et al., 2011; Zhang et al., 2011), appears less sensitive to reductions in Rme-8 than in Vps26, as Wg secretion still occurred in *Rme-8*–depleted tissue. This fits with the model that there is spatial separation of SNX3 and SNX–BAR (containing a Bin/Amphiphysin/Rvs domain) retromer complexes, which may consequently involve different mechanisms (Mari et al., 2008; Harterink et al., 2011; Burd and Cullen, 2014). Recent data have shown that Rme-8 associates with the WASH complex (Freeman et al., 2014), which is involved in the formation/scission of endosomal tubules as well as in cargo recruitment (Seaman et al., 2013; Burd and Cullen, 2014). Our high-resolution microscopy further suggests that Rme-8 could be involved in tubulation of the sorting endosome in a developmental context. Hence, Rme-8 may be specifically required for endosomal routes involving combined actions of retromer and WASH. The possibility that other recycling routes occur independently from Rme-8 would explain why recycling of some receptors, such as the transferrin receptor, still occurs normally when *Rme-8* is knocked down in HeLa cells (Girard and McPherson, 2008).

The ectopic Notch activity in *Rme-8;Vps26* double knockdown was unexpected because neither single knockdown resulted in receptor activation. The activity was independent of Kuz/Adam10, implying that it was ligand independent, as seen for other conditions that result in ectopic Notch activation. Such activation is thought to occur when the receptor remains in the limiting membrane of acidifying endosomes where it can be proteolysed to release NICD (Wilkin et al., 2004, 2008; Hori et al., 2011; Schneider et al., 2013). With the combined depletion of *Vps26* and *Rme-8*, all endocytosed Notch may thus have been routed toward the endolysosomal pathway where some could fail to be incorporated into ILVs, either because it lacked the appropriate modifications or because the volume exceeded the cargo sorting capacity. No such ectopic Notch activity was seen in the absence of *Vps26* alone, suggesting either that the volume of misrouted Notch is higher in the *Rme-8;Vps26*–depleted conditions, for example, if Notch can also be retrieved by Vps26-independent recycling routes that become nonfunctional when *Rme-8* is missing, or that sorting into ILVs is more disrupted when both are depleted.

More dramatic levels of Notch activation occurred when either ESCRT-0 components, *Stam* or *Hrs*, were perturbed in *Rme-8*–depleted cells. Although ESCRT-0 is implicated in sorting ubiquitinylated cargo in preparation for its sequestration into ILVs, no ectopic Notch activation was seen when either or both ESCRT-0 components were missing on their own (Vaccari et al., 2008; Tognon et al., 2014). Furthermore, Hrs removal can even suppress ectopic Notch activity caused by some other trafficking defects (Thompson et al., 2005; Childress et al., 2006; Gallagher and Knoblich, 2006; Jaekel and Klein, 2006; Yamada et al., 2011; Troost et al., 2012). How can these observations be reconciled with the high level of Notch activation in the combined knockdown of *Rme-8* with *Hrs* or *Stam*? One possibility is that, as with the recycling pathway, there are additional Rme-8–dependent mechanisms that sort cargoes into ILVs besides Hrs/Stam. One candidate is SARA, a FYVE domain protein that forms a complex with RNF11 and that has been reported to function in cargo sorting with ESCRT-0 (Kostaras et al., 2013). SARA partially colocalized with Notch in the *Rme-8*–depleted cells and has been associated with Notch activity in some lineages (Coumailleau et al., 2009; Montagne and González-Gaitan, 2014). Another candidate is CD63, a tetraspanin family member implicated in ESCRT-independent sorting of cargoes into ILVs, as well as exosomes (van Niel et al., 2011). Although the function of CD63 homologues has not been explored in *Drosophila*, several tetraspanins affected Notch pathway trafficking or activity in general screens (Dornier et al., 2012; Le Bras et al., 2012). If failure in these, or alternate complexes, can account for the defects brought about by *Rme-8* depletion, it will be interesting to ascertain whether their deployment also involves the WASH complex, making a link between different Rme-8–dependent routes.

Posttranslational modifications also influence ligand-independent Notch activity in the endocytic pathway. In particular, Dx-mediated Notch ubiquitinylation promotes ligand-independent activation by favoring Notch retention in the limiting membrane of MVBs (Hori et al., 2004, 2011; Wilkin et al., 2008; Yamada et al., 2011). However, *Rme-8* depletion did not modify the Dx overexpression phenotypes. This makes it likely that a different pool of Notch is affected and further suggests that not all endolysosomal trafficking routes depend on Rme-8. This may explain the differing consequences of *Rme-8* depletion on other receptor recycling.

Recent discoveries highlight the importance of Rme-8 as a regulatory node in endocytic trafficking. Notably, mutations in *Rme-8* are found in some patients with familial Parkinson's disease where defects in endocytic trafficking are associated with Lewy bodies (Vilariño-Güell et al., 2014). Rme-8 is also among a small cohort of intracellular transport proteins up-regulated in mammal-infective trypanosomes, suggesting it has a role in controlling the copy number of surface proteins (Koumandou et

al., 2013). Here, we have demonstrated its importance in Notch receptor recycling, to maintain adequate levels for signaling, which may also be of relevance for clinical conditions. Furthermore, when combined with defects in Vps26 or ESCRT-0, reductions in Rme-8 enable high levels of ectopic Notch activation, causing tissue hyperplasia and highlighting the potential hazards when such combinatorial mutations arise.

Materials and methods

Drosophila genetics

Further details of the stocks used are provided in Table S1. Knockdown of gene expression was achieved using upstream activation sequence (UAS) Ri lines (Dietzl et al., 2007; Ni et al., 2011) as follows: UAS-*Rme-8-Ri* (Vienna Drosophila Resource Center [VDRC] 22671, 107706), UAS-*w-Ri* (Bloomington Drosophila Stock Center [BL] 35573), UAS-*Su(H)-Ri* (BL 28900), *UAS-Dx-Ri* (VDRC 7795, 106086), UAS-*Vps26-Ri* (VDRC 18396; BL 38937), UAS-*Hrs-Ri* (BL 33900, 34086), and UAS-*Stam-Ri* (VDRC 22497). Additionally, UAS-Kuz^{DN} (BL 6578), UAS-*dx* (Matsuno et al., 2002), and UAS-*Su(dx)* (Cornell et al., 1999) were used for protein expression. Expression of UAS constructs was driven by *en-GAL4,Tub-GAL80*^{ts}, and larvae were shifted to 30°C 24 h after egg laying, except that *Rme-8;ESCRT0* and *Rme-8;Vps26* double knockdowns were shifted to 30°C 72 h after egg laying to avoid lethality. For adult phenotypes, sal^{EPv}*-GAL4* (Cruz et al., 2009) was used, and crosses were maintained at 25°C until adult eclosion.

Mitotic clones were generated using the FRT/FLP system, in which the FLP recombinase induces homologue recombination between FRT (FLP recognition target) sites (Xu and Rubin, 1993). Clones lacking *Rme-8* were obtained using previously characterized x ray–induced loss-of-function alleles whose phenotypes were reportedly rescued by expression of Rme-8 (Chang et al., 2004). Clones were generated by crossing *FRT42D Rme-8C*^{19}*/CyO*, *FRT42D Rme-8*^{A9}*/CyO*, or *Vps35*$^{[MH20]}$ *FRT42D/CyO* (Franch-Marro et al., 2008) to *hsp-FLP122, tub-Gal4, UAS-GFP;tub-Gal80*, *FRT42D GFP/CyO* or to *FRT42D PCNA, Ubi-GFP;hh-flp*. To generate *Hrs* mutant clones, Hrs^{D28} *FRT40A* (Lloyd et al., 2002) was crossed to *hsp-FLP122, tub-Gal4, UAS-GFP;tub-Gal80, FRT40A GFP/CyO*;*NRE-mCherry*. Other lines used include *Gbe+Su(H)-GFP* (*NRE-GFP*) and *Gbe+Su(H)-mCherry* (*NRE-mCherry*; Housden et al., 2012), *tub-Rab4-RFP (*Yousefian et al., 2013*)*, UAS-*FYVE-GFP* (Wucherpfennig et al., 2003), UAS-*Lamp1-GFP* (BL 42714), and *Notch-GFP* (Couturier et al., 2012).

Immunostaining and microscopy

Wing imaginal discs of third-instar larvae were dissected in PBS and fixed in 4% formaldehyde for 20 min. Discs were washed in PBS-DT (0.3% sodium deoxycholate and 0.3% Triton X-100 in PBS) and blocked in BBT (PBS-DT + 1% BSA) before incubation with primary antibodies overnight at 4°C. The following antibodies were used (for further details see Table S2): mouse anti-NICD (1:20; Developmental Studies Hybridoma Bank [DSHB]; Fehon et al., 1990), mouse anti-NECD (1:20; DSHB; Diederich et al., 1994), rat anti-NECD (1:500; Fehon et al., 1990; a gift from S. Artavanis-Tsakonas, Harvard Medical School, Boston, MA), mouse anti-Wg (1:20; DSHB; van den Heuvel et al., 1989), guinea pig anti-Dl (1:3,000; Huppert et al., 1997), rat anti–Cubitus interruptus (Ci; 1:20; DSHB; Motzny and Holmgren, 1995), rabbit anti-GFP (1:1,000; Invitrogen), rabbit anti-dsRed (1:200; Takara Bio Inc.), rabbit anti-Rab7 (1:3,000), and rabbit anti-Rab11 (1:8,000; Tanaka and Nakamura, 2008), guinea pig anti-Hrs (1:1,000; Lloyd et al., 2002; a gift from H. Bellen, Baylor College of Medicine, Houston, TX), rabbit anti-Lva (1:500; Sisson et al., 2000), rabbit anti-Avl (1:1,000; Lu and Bilder, 2005; a gift from D. Bilder, University of California, Berkeley, Berkeley, CA), rabbit anti-Rab5 (1:500; Abcam), guinea pig anti-Vps26 (1:1,000; Wang et al., 2014; a gift from H. Bellen), and rabbit anti-SARA (1:500; Coumailleau et al., 2009). After several washes in PBS-DT, the discs were incubated with fluorescently labeled secondary antibodies, (Jackson ImmunoResearch Laboratories, Inc.; details provided in Table S3), for 1–2 h at RT followed by washing in PBS-DT and labeling with the nuclear marker Hoechst 33342. The samples were mounted in Vectashield (Vector Laboratories) for imaging with D-Eclipse C1 (Plan Fluor 40×, 1.30 NA oil; Plan Apochromat VC 60×, 1.40 NA oil objective lenses; Nikon) or SP2 (63×, 1.40 NA oil objective lens; Leica) confocal microscopes. Samples for high resolution microscopy were stained using Alexa Fluor secondary antibodies and imaged using an OMX-V3 microscope designed by J.W. Sedat (University of California, San Francisco, San Francisco, CA) and built by Applied Precision (Gustafsson et al., 2008). This system uses structured illumination whereby the sample is illuminated with light that has passed through a grating to generate a structured illumination pattern in X, Y, and Z. Three cameras oriented in different angles with respect to the sample collect the emitted light (in total, 15 images/focal plane were acquired). The use of postacquisition algorithms allows reconstruction of the image, giving a resolution below the Abbe limit (~120 nm in X,Y and 350 nm in Z). After acquisition, analysis was performed using ImageJ (National Institutes of Health), a continuous structure over ≥2 focal planes that extended from the main circumference of the endosome was considered to be a "tubule," and the lengths were measured accordingly.

Notch uptake assay

Imaginal discs were dissected in Schneider's *Drosophila* medium and cultured for 1 h at 4°C in the presence of the anti-NECD antibody (1:50; DSHB C458.2H, ascites). After three washes with warm media, discs were incubated at 25°C in Schneider's medium with 200 µM Chloroquine to block lysosomal degradation (100 mM stock in ddH_2O; Sigma-Aldrich). Discs were fixed in 4% formaldehyde at the indicated time points and then incubated with anti-Ci and with the appropriate secondary antibodies to reveal protein localization.

TEM

Wing discs were fixed in 2.5% glutaraldehyde in 100 mM phosphate buffer washed in 100 mM phosphate buffer and postfixed in 2% osmium tetroxide in phosphate buffer for 1 h on ice. After contrasting en bloc in 2% uranyl acetate, the specimens were dehydrated in EtOH and embedded in araldite using acetone as an intermediate solvent. Thin sections were stained with 2% uranyl acetate and lead citrate. Sections were observed under a microscope (EM 902; Carl Zeiss) at 80 kV.

FRAP

For FRAP experiments, WT or *Rme-8*–depleted wing discs expressing Ni-GFP were dissected in culture media (Schneider's *Drosophila* medium supplemented with 2% FBS, 0.5% penicillin-streptavidin, and 0.1 µg/ml Ecdysone (20-hydroxyecdysone; Sigma-Aldrich). Unharmed discs were placed in an observation chamber as previously described (Aldaz et al., 2010) and covered with viscous media (culture media + 2.5× wt/vol methyl-cellulose [Sigma-Aldrich]). For dynasore treatment (Sigma-Aldrich), discs were incubated in Schneider's media containing 100 µM dynasore for 30 min before imaging. Image acquisition was performed using a confocal microscope (FV1000; Olympus) with 100×/1.40 NA oil UPlan-S Apochromat objective lens. Stacks of five z sections spaced by 0.4 µm at a speed of 8 µs/pixel were acquired before and after bleaching and then at 7-s intervals afterward. In each half disc, five circular regions of 0.35-µm radius were photobleached

at apical junctions so that there was only one bleach event per cell. Photobleaching was performed with 10 scans at 8 µs/pixel, using 100% 488-nm laser power. For each field, three background, five control regions, and five bleached regions were measured over time, and intensities were calculated using ImageJ. Mean fluorescent intensities from background were subtracted from the mean control and mean bleached datasets, and, to normalize for fluorescence changes during imaging, the bleached regions were then normalized to controls. At least two fields of view were analyzed per disc, and 10–12 discs were analyzed per dataset. As described previously for experiments analyzing Cadherin (Bulgakova et al., 2013), each dataset was fitted to a biexponential of the form $f(t) = 1 - F_{im} - A^1 \times e^{-t/T}\text{fast} - A^2 \times e^{-t/T}\text{slow}$ and to a single exponential of the form $f(t) = 1 - F_{im} - A^1 \times e^{-t/T}\text{fast}$, where F_{im} is a size of the immobile pool of the protein, ^{T}fast and ^{T}slow are the half-times, and A^1 and A^2 are the amplitudes of the fast and slow components of the recovery. An F test was used to assess which of the equations better described each dataset. For recovery curves in WT or *Rme-8*–depleted tissues, the biexponential equation gave the better fit, and the resulting p-values are indicated.

Online supplemental material

Fig. S1 shows *Rme-8 Ri* knockdown and phenotypes. Fig. S2 shows that *Rme-8* appears to regulate Notch trafficking independently of Dx and Su(dx). Fig. S3 shows that Notch associates with enlarged endosomes. Fig. S4 shows TEM analysis of *Rme-8, Hrs*, and *Vps26* knockdowns. Fig. S5 shows retromer and ESCRT-0 Ri validation and phenotypes. Table S1 gives details of *Drosophila* strains. Table S2 gives details of primary antibodies. Table S3 gives details of secondary antibodies. Online supplemental material is available at http://www.jcb.org/cgi/content/full/jcb.201411001/DC1.

Acknowledgements

We thank N. Bulgakova for assistance with FRAP experiments, N. Lawrence for help with OMX-V3, T. Vaccari (l'Istituto FIRC di Oncologia Molecolare, Milan, Italy) for guidance with the uptake assay, H. Bellen (Baylor College of Medicine, Houston, TX), D. Bilder (University of California, Berkeley, Berkeley, CA), J.-P. Vincent (National Institute for Medical Research, London, England, UK), and S. Artavanis-Tsakonas (Harvard Medical School, Boston, MA) for sharing reagents. We thank TRiP (Transgenic RNAi Project) at Harvard Medical School (National Institutes of Health/National Institute of General Medical Sciences R01-GM084947) and VDRC (Vienna, Austria) for transgenic Ri flies used in this study.

This work was funded by a Medical Research Council program grant (G0800034) to S.J. Bray. L.A. Snowden was the recipient of a Biotechnology and Biological Sciences Research Council PhD studentship. E. Seib and T. Klein were funded by the Deutsche Forschungsgemeinschaft (Sachbeihilfe KL 1028/5-1).

The authors declare no competing financial interests.

Submitted: 3 November 2014
Accepted: 11 June 2015

References

Aldaz, S., L.M. Escudero, and M. Freeman. 2010. Live imaging of *Drosophila* imaginal disc development. *Proc. Natl. Acad. Sci. USA.* 107:14217–14222. http://dx.doi.org/10.1073/pnas.1008623107

Baron, M. 2012. Endocytic routes to Notch activation. *Semin. Cell Dev. Biol.* 23:437–442. http://dx.doi.org/10.1016/j.semcdb.2012.01.008

Belenkaya, T.Y., Y. Wu, X. Tang, B. Zhou, L. Cheng, Y.V. Sharma, D. Yan, E.M. Selva, and X. Lin. 2008. The retromer complex influences Wnt secretion by recycling wntless from endosomes to the trans-Golgi network. *Dev. Cell.* 14:120–131. http://dx.doi.org/10.1016/j.devcel.2007.12.003

Bray, S.J. 2006. Notch signalling: a simple pathway becomes complex. *Nat. Rev. Mol. Cell Biol.* 7:678–689. http://dx.doi.org/10.1038/nrm2009

Brou, C. 2009. Intracellular trafficking of Notch receptors and ligands. *Exp. Cell Res.* 315:1549–1555. http://dx.doi.org/10.1016/j.yexcr.2008.09.010

Bulgakova, N.A., I. Grigoriev, A.S. Yap, A. Akhmanova, and N.H. Brown. 2013. Dynamic microtubules produce an asymmetric E-cadherin–Bazooka complex to maintain segment boundaries. *J. Cell Biol.* 201:887–901. http://dx.doi.org/10.1083/jcb.201211159

Burd, C., and P.J. Cullen. 2014. Retromer: a master conductor of endosome sorting. *Cold Spring Harb. Perspect. Biol.* 6:6. http://dx.doi.org/10.1101/cshperspect.a016774

Chang, H.C., M. Hull, and I. Mellman. 2004. The J-domain protein Rme-8 interacts with Hsc70 to control clathrin-dependent endocytosis in *Drosophila*. *J. Cell Biol.* 164:1055–1064. http://dx.doi.org/10.1083/jcb.200311084

Childress, J.L., M. Acar, C. Tao, and G. Halder. 2006. Lethal giant discs, a novel C2-domain protein, restricts notch activation during endocytosis. *Curr. Biol.* 16:2228–2233. http://dx.doi.org/10.1016/j.cub.2006.09.031

Cohen, M., M. Georgiou, N.L. Stevenson, M. Miodownik, and B. Baum. 2010. Dynamic filopodia transmit intermittent Delta-Notch signaling to drive pattern refinement during lateral inhibition. *Dev. Cell.* 19:78–89. http://dx.doi.org/10.1016/j.devcel.2010.06.006

Cornell, M., D.A. Evans, R. Mann, M. Fostier, M. Flasza, M. Monthatong, S. Artavanis-Tsakonas, and M. Baron. 1999. The *Drosophila melanogaster* Suppressor of deltex gene, a regulator of the Notch receptor signaling pathway, is an E3 class ubiquitin ligase. *Genetics.* 152:567–576.

Coumailleau, F., M. Fürthauer, J.A. Knoblich, and M. González-Gaitán. 2009. Directional Delta and Notch trafficking in Sara endosomes during asymmetric cell division. *Nature.* 458:1051–1055. http://dx.doi.org/10.1038/nature07854

Couturier, L., N. Vodovar, and F. Schweisguth. 2012. Endocytosis by Numb breaks Notch symmetry at cytokinesis. *Nat. Cell Biol.* 14:131–139. http://dx.doi.org/10.1038/ncb2419

Cruz, C., A. Glavic, M. Casado, and J.F. de Celis. 2009. A gain-of-function screen identifying genes required for growth and pattern formation of the *Drosophila melanogaster* wing. *Genetics.* 183:1005–1026. http://dx.doi.org/10.1534/genetics.109.107748

de Celis, J.F., and S. Bray. 1997. Feed-back mechanisms affecting Notch activation at the dorsoventral boundary in the *Drosophila* wing. *Development.* 124:3241–3251.

de Joussineau, C., J. Soulé, M. Martin, C. Anguille, P. Montcourrier, and D. Alexandre. 2003. Delta-promoted filopodia mediate long-range lateral inhibition in *Drosophila*. *Nature.* 426:555–559. http://dx.doi.org/10.1038/nature02157

Diederich, R.J., K. Matsuno, H. Hing, and S. Artavanis-Tsakonas. 1994. Cytosolic interaction between deltex and Notch ankyrin repeats implicates deltex in the Notch signaling pathway. *Development.* 120:473–481.

Dietzl, G., D. Chen, F. Schnorrer, K.C. Su, Y. Barinova, M. Fellner, B. Gasser, K. Kinsey, S. Oppel, S. Scheiblauer, et al. 2007. A genome-wide transgenic RNAi library for conditional gene inactivation in *Drosophila*. *Nature.* 448:151–156. http://dx.doi.org/10.1038/nature05954

Dornier, E., F. Coumailleau, J.F. Ottavi, J. Moretti, C. Boucheix, P. Mauduit, F. Schweisguth, and E. Rubinstein. 2012. TspanC8 tetraspanins regulate ADAM10/Kuzbanian trafficking and promote Notch activation in flies and mammals. *J. Cell Biol.* 199:481–496. http://dx.doi.org/10.1083/jcb.201201133

Fabrowski, P., A.S. Necakov, S. Mumbauer, E. Loeser, A. Reversi, S. Streichan, J.A. Briggs, and S. De Renzis. 2013. Tubular endocytosis drives remodelling of the apical surface during epithelial morphogenesis in *Drosophila*. *Nat. Commun.* 4:2244. http://dx.doi.org/10.1038/ncomms3244

Fehon, R.G., P.J. Kooh, I. Rebay, C.L. Regan, T. Xu, M.A.T. Muskavitch, and S. Artavanis-Tsakonas. 1990. Molecular interactions between the protein products of the neurogenic loci Notch and Delta, two EGF-homologous genes in *Drosophila. Cell.* 61:523–534. http://dx.doi.org/10.1016/0092-8674(90)90534-L

Fortini, M.E., and D. Bilder. 2009. Endocytic regulation of Notch signaling. *Curr. Opin. Genet. Dev.* 19:323–328. http://dx.doi.org/10.1016/j.gde.2009.04.005

Franch-Marro, X., F. Wendler, S. Guidato, J. Griffith, A. Baena-Lopez, N. Itasaki, M.M. Maurice, and J.-P. Vincent. 2008. Wingless secretion requires endosome-to-Golgi retrieval of Wntless/Evi/Sprinter by the retromer complex. *Nat. Cell Biol.* 10:170–177. http://dx.doi.org/10.1038/ncb1678

Freeman, C.L., G. Hesketh, and M.N.J. Seaman. 2014. RME-8 coordinates the activity of the WASH complex with the function of the retromer SNX

dimer to control endosomal tubulation. *J. Cell Sci.* 127:2053–2070. http://dx.doi.org/10.1242/jcs.144659

Fujibayashi, A., T. Taguchi, R. Misaki, M. Ohtani, N. Dohmae, K. Takio, M. Yamada, J. Gu, M. Yamakami, M. Fukuda, et al. 2008. Human RME-8 is involved in membrane trafficking through early endosomes. *Cell Struct. Funct.* 33:35–50. http://dx.doi.org/10.1247/csf.07045

Gallagher, C.M., and J.A. Knoblich. 2006. The conserved c2 domain protein lethal (2) giant discs regulates protein trafficking in *Drosophila*. *Dev. Cell.* 11:641–653. http://dx.doi.org/10.1016/j.devcel.2006.09.014

Girard, M., and P.S. McPherson. 2008. RME-8 regulates trafficking of the epidermal growth factor receptor. *FEBS Lett.* 582:961–966. http://dx.doi.org/10.1016/j.febslet.2008.02.042

Girard, M., V. Poupon, F. Blondeau, and P.S. McPherson. 2005. The DnaJ-domain protein RME-8 functions in endosomal trafficking. *J. Biol. Chem.* 280:40135–40143. http://dx.doi.org/10.1074/jbc.M505036200

Grant, B.D., and J.G. Donaldson. 2009. Pathways and mechanisms of endocytic recycling. *Nat. Rev. Mol. Cell Biol.* 10:597–608. http://dx.doi.org/10.1038/nrm2755

Gustafsson, M.G., L. Shao, P.M. Carlton, C.J. Wang, I.N. Golubovskaya, W.Z. Cande, D.A. Agard, and J.W. Sedat. 2008. Three-dimensional resolution doubling in wide-field fluorescence microscopy by structured illumination. *Biophys. J.* 94:4957–4970. http://dx.doi.org/10.1529/biophysj.107.120345

Hanyaloglu, A.C., E. McCullagh, and M. von Zastrow. 2005. Essential role of Hrs in a recycling mechanism mediating functional resensitization of cell signaling. *EMBO J.* 24:2265–2283. http://dx.doi.org/10.1038/sj.emboj.7600688

Harterink, M., F. Port, M.J. Lorenowicz, I.J. McGough, M. Silhankova, M.C. Betist, J.R.T. van Weering, R.G.H.P. van Heesbeen, T.C. Middelkoop, K. Basler, et al. 2011. A SNX3-dependent retromer pathway mediates retrograde transport of the Wnt sorting receptor Wntless and is required for Wnt secretion. *Nat. Cell Biol.* 13:914–923. http://dx.doi.org/10.1038/ncb2281

Henne, W.M., N.J. Buchkovich, and S.D. Emr. 2011. The ESCRT pathway. *Dev. Cell.* 21:77–91. http://dx.doi.org/10.1016/j.devcel.2011.05.015

Hori, K., M. Fostier, M. Ito, T.J. Fuwa, M.J. Go, H. Okano, M. Baron, and K. Matsuno. 2004. *Drosophila* deltex mediates suppressor of Hairless-independent and late-endosomal activation of Notch signaling. *Development.* 131:5527–5537. http://dx.doi.org/10.1242/dev.01448

Hori, K., A. Sen, T. Kirchhausen, and S. Artavanis-Tsakonas. 2011. Synergy between the ESCRT-III complex and Deltex defines a ligand-independent Notch signal. *J. Cell Biol.* 195:1005–1015. http://dx.doi.org/10.1083/jcb.201104146

Housden, B.E., K. Millen, and S.J. Bray. 2012. *Drosophila* reporter vectors compatible with ΦC31 integrase transgenesis techniques and their use to generate new Notch reporter fly lines. *G3 (Bethesda).* 2:79–82. http://dx.doi.org/10.1534/g3.111.001321

Huppert, S.S., T.L. Jacobsen, and M.A. Muskavitch. 1997. Feedback regulation is central to Delta-Notch signalling required for *Drosophila* wing vein morphogenesis. *Development.* 124:3283–3291.

Hurley, J.H., and S.D. Emr. 2006. The ESCRT complexes: structure and mechanism of a membrane-trafficking network. *Annu. Rev. Biophys. Biomol. Struct.* 35:277–298. http://dx.doi.org/10.1146/annurev.biophys.35.040405.102126

Jaekel, R., and T. Klein. 2006. The *Drosophila* Notch inhibitor and tumor suppressor gene lethal (2) giant discs encodes a conserved regulator of endosomal trafficking. *Dev. Cell.* 11:655–669. http://dx.doi.org/10.1016/j.devcel.2006.09.019

Jovic, M., M. Sharma, J. Rahajeng, and S. Caplan. 2010. The early endosome: a busy sorting station for proteins at the crossroads. *Histol. Histopathol.* 25:99–112.

Kostaras, E., G. Sflomos, N.M. Pedersen, H. Stenmark, T. Fotsis, and C. Murphy. 2013. SARA and RNF11 interact with each other and ESCRT-0 core proteins and regulate degradative EGFR trafficking. *Oncogene.* 32:5220–5232. http://dx.doi.org/10.1038/onc.2012.554

Koumandou, V.L., C. Boehm, K.A. Horder, and M.C. Field. 2013. Evidence for recycling of invariant surface transmembrane domain proteins in African trypanosomes. *Eukaryot. Cell.* 12:330–342. http://dx.doi.org/10.1128/EC.00273-12

Le Borgne, R., and F. Schweisguth. 2003. Unequal segregation of Neuralized biases Notch activation during asymmetric cell division. *Dev. Cell.* 5:139–148. http://dx.doi.org/10.1016/S1534-5807(03)00187-4

Le Bras, S., C. Rondanino, G. Kriegel-Taki, A. Dussert, and R. Le Borgne. 2012. Genetic identification of intracellular trafficking regulators involved in Notch-dependent binary cell fate acquisition following asymmetric cell division. *J. Cell Sci.* 125:4886–4901. http://dx.doi.org/10.1242/jcs.110171

Li, H., H.-F. Li, R.A. Felder, A. Periasamy, and P.A. Jose. 2008. Rab4 and Rab11 coordinately regulate the recycling of angiotensin II type I receptor as demonstrated by fluorescence resonance energy transfer microscopy. *J. Biomed. Opt.* 13:031206. http://dx.doi.org/10.1117/1.2943286

Lloyd, T.E., R. Atkinson, M.N. Wu, Y. Zhou, G. Pennetta, and H.J. Bellen. 2002. Hrs regulates endosome membrane invagination and tyrosine kinase receptor signaling in *Drosophila*. *Cell.* 108:261–269. http://dx.doi.org/10.1016/S0092-8674(02)00611-6

Lobry, C., P. Oh, and I. Aifantis. 2011. Oncogenic and tumor suppressor functions of Notch in cancer: it's NOTCH what you think. *J. Exp. Med.* 208:1931–1935. http://dx.doi.org/10.1084/jem.20111855

Lu, H., and D. Bilder. 2005. Endocytic control of epithelial polarity and proliferation in *Drosophila*. *Nat. Cell Biol.* 7:1232–1239. http://dx.doi.org/10.1038/ncb1324

Mari, M., M.V. Bujny, D. Zeuschner, W.J.C. Geerts, J. Griffith, C.M. Petersen, P.J. Cullen, J. Klumperman, and H.J. Geuze. 2008. SNX1 defines an early endosomal recycling exit for sortilin and mannose 6-phosphate receptors. *Traffic.* 9:380–393. http://dx.doi.org/10.1111/j.1600-0854.2007.00686.x

Matsuno, K., M. Ito, K. Hori, F. Miyashita, S. Suzuki, N. Kishi, S. Artavanis-Tsakonas, and H. Okano. 2002. Involvement of a proline-rich motif and RING-H2 finger of Deltex in the regulation of Notch signaling. *Development.* 129:1049–1059.

McGough, I.J., and P.J. Cullen. 2011. Recent advances in retromer biology. *Traffic.* 12:963–971. http://dx.doi.org/10.1111/j.1600-0854.2011.01201.x

McGough, I.J., F. Steinberg, D. Jia, P.A. Barbuti, K.J. McMillan, K.J. Heesom, A.L. Whone, M.A. Caldwell, D.D. Billadeau, M.K. Rosen, and P.J. Cullen. 2014. Retromer binding to FAM21 and the WASH complex is perturbed by the Parkinson disease-linked VPS35(D620N) mutation. *Curr. Biol.* 24:1670–1676. http://dx.doi.org/10.1016/j.cub.2014.06.024

Millman, E.E., H. Zhang, H. Zhang, V. Godines, A.J. Bean, B.J. Knoll, and R.H. Moore. 2008. Rapid recycling of β-adrenergic receptors is dependent on the actin cytoskeleton and myosin Vb. *Traffic.* 9:1958–1971. http://dx.doi.org/10.1111/j.1600-0854.2008.00813.x

Miura, E., T. Hasegawa, M. Konno, M. Suzuki, N. Sugeno, N. Fujikake, S. Geisler, M. Tabuchi, R. Oshima, A. Kikuchi, et al. 2014. VPS35 dysfunction impairs lysosomal degradation of α-synuclein and exacerbates neurotoxicity in a *Drosophila* model of Parkinson's disease. *Neurobiol. Dis.* 71:1–13. http://dx.doi.org/10.1016/j.nbd.2014.07.014

Moberg, K.H., S. Schelble, S.K. Burdick, and I.K. Hariharan. 2005. Mutations in erupted, the *Drosophila* ortholog of mammalian tumor susceptibility gene 101, elicit non-cell-autonomous overgrowth. *Dev. Cell.* 9:699–710. http://dx.doi.org/10.1016/j.devcel.2005.09.018

Montagne, C., and M. González-Gaitan. 2014. Sara endosomes and the asymmetric division of intestinal stem cells. *Development.* 141:2014–2023. http://dx.doi.org/10.1242/dev.104240

Morrison, H.A., H. Dionne, T.E. Rusten, A. Brech, W.W. Fisher, B.D. Pfeiffer, S.E. Celniker, H. Stenmark, and D. Bilder. 2008. Regulation of early endosomal entry by the *Drosophila* tumor suppressors Rabenosyn and Vps45. *Mol. Biol. Cell.* 19:4167–4176. http://dx.doi.org/10.1091/mbc.E08-07-0716

Motzny, C.K., and R. Holmgren. 1995. The *Drosophila* cubitus interruptus protein and its role in the wingless and hedgehog signal transduction pathways. *Mech. Dev.* 52:137–150. http://dx.doi.org/10.1016/0925-4773(95)00397-J

Ni, J.Q., R. Zhou, B. Czech, L.P. Liu, L. Holderbaum, D. Yang-Zhou, H.S. Shim, R. Tao, D. Handler, P. Karpowicz, et al. 2011. A genome-scale shRNA resource for transgenic RNAi in *Drosophila*. *Nat. Methods.* 8:405–407. http://dx.doi.org/10.1038/nmeth.1592

Nolo, R., L.A. Abbott, and H.J. Bellen. 2000. Senseless, a Zn finger transcription factor, is necessary and sufficient for sensory organ development in *Drosophila*. *Cell.* 102:349–362. http://dx.doi.org/10.1016/S0092-8674(00)00040-4

Pan, C.L., P.D. Baum, M. Gu, E.M. Jorgensen, S.G. Clark, and G. Garriga. 2008. *C. elegans* AP-2 and retromer control Wnt signaling by regulating mig-14/Wntless. *Dev. Cell.* 14:132–139. http://dx.doi.org/10.1016/j.devcel.2007.12.001

Piddini, E., F. Marshall, L. Dubois, E. Hirst, and J.P. Vincent. 2005. Arrow (LRP6) and Frizzled2 cooperate to degrade Wingless in *Drosophila* imaginal discs. *Development.* 132:5479–5489. http://dx.doi.org/10.1242/dev.02145

Pocha, S.M., T. Wassmer, C. Niehage, B. Hoflack, and E. Knust. 2011. Retromer controls epithelial cell polarity by trafficking the apical determinant Crumbs. *Curr. Biol.* 21:1111–1117. http://dx.doi.org/10.1016/j.cub.2011.05.007

Popoff, V., G.A. Mardones, S.-K. Bai, V. Chambon, D. Tenza, P.V. Burgos, A. Shi, P. Benaroch, S. Urbé, C. Lamaze, et al. 2009. Analysis of articulation between clathrin and retromer in retrograde sort-

ing on early endosomes. *Traffic.* 10:1868–1880. http://dx.doi.org/10.1111/j.1600-0854.2009.00993.x

Port, F., M. Kuster, P. Herr, E. Furger, C. Bänziger, G. Hausmann, and K. Basler. 2008. Wingless secretion promotes and requires retromer-dependent cycling of Wntless. *Nat. Cell Biol.* 10:178–185. http://dx.doi.org/10.1038/ncb1687

Rives, A.F., K.M. Rochlin, M. Wehrli, S.L. Schwartz, and S. DiNardo. 2006. Endocytic trafficking of Wingless and its receptors, Arrow and DFrizzled-2, in the *Drosophila* wing. *Dev. Biol.* 293:268–283. http://dx.doi.org/10.1016/j.ydbio.2006.02.006

Schneider, M., T. Troost, F. Grawe, A. Martinez-Arias, and T. Klein. 2013. Activation of Notch in lgd mutant cells requires the fusion of late endosomes with the lysosome. *J. Cell Sci.* 126:645–656. http://dx.doi.org/10.1242/jcs.116590

Seaman, M.N.J. 2012. The retromer complex - endosomal protein recycling and beyond. *J. Cell Sci.* 125:4693–4702. http://dx.doi.org/10.1242/jcs.103440

Seaman, M.N.J., A. Gautreau, and D.D. Billadeau. 2013. Retromer-mediated endosomal protein sorting: all WASHed up! *Trends Cell Biol.* 23:522–528. http://dx.doi.org/10.1016/j.tcb.2013.04.010

Shi, A., L. Sun, R. Banerjee, M. Tobin, Y. Zhang, and B.D. Grant. 2009. Regulation of endosomal clathrin and retromer-mediated endosome to Golgi retrograde transport by the J-domain protein RME-8. *EMBO J.* 28:3290–3302. http://dx.doi.org/10.1038/emboj.2009.272

Sisson, J.C., C. Field, R. Ventura, A. Royou, and W. Sullivan. 2000. Lava lamp, a novel peripheral golgi protein, is required for *Drosophila melanogaster* cellularization. *J. Cell Biol.* 151:905–918. http://dx.doi.org/10.1083/jcb.151.4.905

Sönnichsen, B., S. De Renzis, E. Nielsen, J. Rietdorf, and M. Zerial. 2000. Distinct membrane domains on endosomes in the recycling pathway visualized by multicolor imaging of Rab4, Rab5, and Rab11. *J. Cell Biol.* 149:901–914. http://dx.doi.org/10.1083/jcb.149.4.901

Sprinzak, D., A. Lakhanpal, L. Lebon, L.A. Santat, M.E. Fontes, G.A. Anderson, J. Garcia-Ojalvo, and M.B. Elowitz. 2010. Cis-interactions between Notch and Delta generate mutually exclusive signalling states. *Nature.* 465:86–90. http://dx.doi.org/10.1038/nature08959

Steinberg, F., M. Gallon, M. Winfield, E.C. Thomas, A.J. Bell, K.J. Heesom, J.M. Tavaré, and P.J. Cullen. 2013. A global analysis of SNX27-retromer assembly and cargo specificity reveals a function in glucose and metal ion transport. *Nat. Cell Biol.* 15:461–471. http://dx.doi.org/10.1038/ncb2721

Tanaka, T., and A. Nakamura. 2008. The endocytic pathway acts downstream of Oskar in *Drosophila* germ plasm assembly. *Development.* 135:1107–1117. http://dx.doi.org/10.1242/dev.017293

Temkin, P., B. Lauffer, S. Jäger, P. Cimermancic, N.J. Krogan, and M. von Zastrow. 2011. SNX27 mediates retromer tubule entry and endosome-to-plasma membrane trafficking of signalling receptors. *Nat. Cell Biol.* 13:715–721. http://dx.doi.org/10.1038/ncb2252

Thompson, B.J., J. Mathieu, H.-H. Sung, E. Loeser, P. Rørth, and S.M. Cohen. 2005. Tumor suppressor properties of the ESCRT-II complex component Vps25 in *Drosophila*. *Dev. Cell.* 9:711–720. http://dx.doi.org/10.1016/j.devcel.2005.09.020

Tognon, E., N. Wollscheid, K. Cortese, C. Tacchetti, and T. Vaccari. 2014. ESCRT-0 is not required for ectopic Notch activation and tumor suppression in *Drosophila*. *PLoS ONE.* 9:e93987. http://dx.doi.org/10.1371/journal.pone.0093987

Troost, T., S. Jaeckel, N. Ohlenhard, and T. Klein. 2012. The tumour suppressor Lethal (2) giant discs is required for the function of the ESCRT-III component Shrub/CHMP4. *J. Cell Sci.* 125:763–776. http://dx.doi.org/10.1242/jcs.097261

Vaccari, T., and D. Bilder. 2005. The *Drosophila* tumor suppressor vps25 prevents nonautonomous overproliferation by regulating notch trafficking. *Dev. Cell.* 9:687–698. http://dx.doi.org/10.1016/j.devcel.2005.09.019

Vaccari, T., H. Lu, R. Kanwar, M.E. Fortini, and D. Bilder. 2008. Endosomal entry regulates Notch receptor activation in *Drosophila melanogaster*. *J. Cell Biol.* 180:755–762. http://dx.doi.org/10.1083/jcb.200708127

Vaccari, T., T.E. Rusten, L. Menut, I.P. Nezis, A. Brech, H. Stenmark, and D. Bilder. 2009. Comparative analysis of ESCRT-I, ESCRT-II and ESCRT-III function in *Drosophila* by efficient isolation of ESCRT mutants. *J. Cell Sci.* 122:2413–2423. http://dx.doi.org/10.1242/jcs.046391

van den Heuvel, M., R. Nusse, P. Johnston, and P.A. Lawrence. 1989. Distribution of the wingless gene product in *Drosophila* embryos: a protein involved in cell-cell communication. *Cell.* 59:739–749. http://dx.doi.org/10.1016/0092-8674(89)90020-2

van Niel, G., S. Charrin, S. Simoes, M. Romao, L. Rochin, P. Saftig, M.S. Marks, E. Rubinstein, and G. Raposo. 2011. The tetraspanin CD63 regulates ESCRT-independent and -dependent endosomal sorting during melanogenesis. *Dev. Cell.* 21:708–721. http://dx.doi.org/10.1016/j.devcel.2011.08.019

Vilariño-Güell, C., C. Wider, O.A. Ross, J.C. Dachsel, J.M. Kachergus, S.J. Lincoln, A.I. Soto-Ortolaza, S.A. Cobb, G.J. Wilhoite, J.A. Bacon, et al. 2011. VPS35 mutations in Parkinson disease. *Am. J. Hum. Genet.* 89:162–167. http://dx.doi.org/10.1016/j.ajhg.2011.06.001

Vilariño-Güell, C., A. Rajput, A.J. Milnerwood, B. Shah, C. Szu-Tu, J. Trinh, I. Yu, M. Encarnacion, L.N. Munsie, L. Tapia, et al. 2014. DNAJC13 mutations in Parkinson disease. *Hum. Mol. Genet.* 23:1794–1801. http://dx.doi.org/10.1093/hmg/ddt570

Wang, S., K.L. Tan, M.A. Agosto, B. Xiong, S. Yamamoto, H. Sandoval, M. Jaiswal, V. Bayat, K. Zhang, W.-L. Charng, et al. 2014. The retromer complex is required for rhodopsin recycling and its loss leads to photoreceptor degeneration. *PLoS Biol.* 12:e1001847. http://dx.doi.org/10.1371/journal.pbio.1001847

Wilkin, M.B., A.-M. Carbery, M. Fostier, H. Aslam, S.L. Mazaleyrat, J. Higgs, A. Myat, D.A.P. Evans, M. Cornell, and M. Baron. 2004. Regulation of notch endosomal sorting and signaling by *Drosophila* Nedd4 family proteins. *Curr. Biol.* 14:2237–2244. http://dx.doi.org/10.1016/j.cub.2004.11.030

Wilkin, M., P. Tongngok, N. Gensch, S. Clemence, M. Motoki, K. Yamada, K. Hori, M. Taniguchi-Kanai, E. Franklin, K. Matsuno, and M. Baron. 2008.*Drosophila* HOPS and AP-3 complex genes are required for a Deltex-regulated activation of notch in the endosomal trafficking pathway. *Dev. Cell.* 15:762–772. http://dx.doi.org/10.1016/j.devcel.2008.09.002

Wucherpfennig, T., M. Wilsch-Bräuninger, and M. González-Gaitán. 2003. Role of *Drosophila* Rab5 during endosomal trafficking at the synapse and evoked neurotransmitter release. *J. Cell Biol.* 161:609–624. http://dx.doi.org/10.1083/jcb.200211087

Xu, T., and G.M. Rubin. 1993. Analysis of genetic mosaics in developing and adult *Drosophila* tissues. *Development.* 117:1223–1237.

Yamada, K., T.J. Fuwa, T. Ayukawa, T. Tanaka, A. Nakamura, M.B. Wilkin, M. Baron, and K. Matsuno. 2011. Roles of *Drosophila* deltex in Notch receptor endocytic trafficking and activation. *Genes Cells.* 16:261–272. http://dx.doi.org/10.1111/j.1365-2443.2011.01488.x

Yan, Q., W. Sun, P. Kujala, Y. Lotfi, T.A. Vida, and A.J. Bean. 2005. CART: an Hrs/actinin-4/BERP/myosin V protein complex required for efficient receptor recycling. *Mol. Biol. Cell.* 16:2470–2482. http://dx.doi.org/10.1091/mbc.E04-11-1014

Yang, P.T., M.J. Lorenowicz, M. Silhankova, D.Y. Coudreuse, M.C. Betist, and H.C. Korswagen. 2008. Wnt signaling requires retromer-dependent recycling of MIG-14/Wntless in Wnt-producing cells. *Dev. Cell.* 14:140–147. http://dx.doi.org/10.1016/j.devcel.2007.12.004

Yousefian, J., T. Troost, F. Grawe, T. Sasamura, M. Fortini, and T. Klein. 2013. Dmon1 controls recruitment of Rab7 to maturing endosomes in *Drosophila*. *J. Cell Sci.* 126:1583–1594. http://dx.doi.org/10.1242/jcs.114934

Zavodszky, E., M.N. Seaman, K. Moreau, M. Jimenez-Sanchez, S.Y. Breusegem, M.E. Harbour, and D.C. Rubinsztein. 2014. Mutation in VPS35 associated with Parkinson's disease impairs WASH complex association and inhibits autophagy. *Nat. Commun.* 5:3828. http://dx.doi.org/10.1038/ncomms4828

Zhang, Y., B. Grant, and D. Hirsh. 2001. RME-8, a conserved J-domain protein, is required for endocytosis in *Caenorhabditis elegans*. *Mol. Biol. Cell.* 12:2011–2021. http://dx.doi.org/10.1091/mbc.12.7.2011

Zhang, P., Y. Wu, T.Y. Belenkaya, and X. Lin. 2011. SNX3 controls Wingless/Wnt secretion through regulating retromer-dependent recycling of Wntless. *Cell Res.* 21:1677–1690. http://dx.doi.org/10.1038/cr.2011.167

Zimprich, A., A. Benet-Pagès, W. Struhal, E. Graf, S.H. Eck, M.N. Offman, D. Haubenberger, S. Spielberger, E.C. Schulte, P. Lichtner, et al. 2011. A mutation in VPS35, encoding a subunit of the retromer complex, causes late-onset Parkinson disease. *Am. J. Hum. Genet.* 89:168–175. http://dx.doi.org/10.1016/j.ajhg.2011.06.008